

University of Alberta

Arsenic effects on a NiMo/Al₂O₃ hydrotreating catalyst

by

Paola Scholte

A thesis submitted to the Faculty of Graduate Studies and Research
in partial fulfillment of the requirements for the degree of

Master of Science

in

Chemical Engineering

Department of Chemical and Materials Engineering

©Paola Scholte

Spring 2011

Edmonton, Alberta

Permission is hereby granted to the University of Alberta Libraries to reproduce single copies of this thesis and to lend or sell such copies for private, scholarly or scientific research purposes only. Where the thesis is converted to, or otherwise made available in digital form, the University of Alberta will advise potential users of the thesis of these terms.

The author reserves all other publication and other rights in association with the copyright in the thesis and, except as herein before provided, neither the thesis nor any substantial portion thereof may be printed or otherwise reproduced in any material form whatsoever without the author's prior written permission.

Abstract

Hydrotreating is the response to the necessity of a cleaner feed for downstream processes and reduced pollution. Hydrotreating catalysts are vital in this process; hence catalyst deactivation is a key issue. The principal objective of this research was the experimental study of hydrotreating catalyst deactivation due to arsenic compounds. The hydrotreating of light gas oil, in the presence and absence of an arsenic compound over a commercial NiMoS catalyst, was investigated in a trickle bed reactor (temperature 315-360°C, space velocity = 1-3 h⁻¹, pressure = 3MPa). Kinetics of first order for nitrogen and sulphur were found and activation energies values of 32 kJ/mol and 76 kJ/mol respectively. Studies of activity changes, suggested that arsenic mainly affects the conversion of sulfur compounds; which might indicate that arsenic prefers mainly the S edge of the catalysts. Activation energy values decreased after arsenic introduction, which may suggest pore plugging of the catalyst.

Acknowledgments

The most sincere appreciation to my supervisor, Dr. William McCaffrey, for his support and thoughtful guidance throughout this research. Thank you for your patience and for sharing your knowledge and experience with me. Thanks for everything!!!

I express my gratitude to Shaofeng Yang, who was a great support through the whole research. Thank you for your great help during difficult days at the lab.

I appreciate the help of Dr Adjaye for supplying the catalyst, the light gas oil feed and valuable information during the project.

Special thanks to Syncrude Canada Ltd and the National Sciences and Engineering Research Council of Canada (NSERC) for providing financial support for this project.

I sincerely thank to my family and friends for their support, love, faith and patience during the development of this research.

Thank you!

Table of Contents

Chapter 1	Introduction	1
Chapter 2	Literature Review	4
2.1.1	Hydrotreating	4
2.1.2	Hydrodesulfuration	5
2.1.3	Hydrodenitrogenation	6
2.1.4	Hydrodemetallation	8
2.2	Hydrotreating catalyst	11
2.2.1	Catalyst deactivation	13
2.3	Trickle bed reactor hydrodynamics	16
2.3.1	Liquid hold up	16
2.3.2	Catalyst wetting	18
2.3.3	Axial dispersion	19
Chapter 3	Materials and methods	22
3.1	Materials and chemicals	22
3.2	Experimental equipment	23
3.2.1	Hydrogen feed line	24
3.2.2	Liquid feed line	25
3.2.3	Reactor	25
3.2.4	Pressure control system	27
3.2.5	Argon, Nitrogen, hydrogen sulphide and hydrogen feed line	29
3.2.6	Liquid product feed line	30

3.3	Experimental procedure	31
3.3.1	Reactor loading	31
3.3.2	Pressure leak test	33
3.3.3	Reactor startup, experimental operation and shut down	34
3.3.4	Catalyst sulfidation	38
3.3.5	Reactor and system saturation	38
3.3.6	Liquid sample analysis	38
3.3.7	Catalyst analysis	39
3.4	Safety Measures	40
Chapter 4	Results and discussions	42
4.1	Determination of the residence time	42
4.2	Reactor operation improvement	45
4.2.1	Pressure and temperature management	45
4.3	Kinetics of sulphur and nitrogen removal	49
4.3.1	Effects of LHSV and temperature on HDS and HDN	50
4.4	Arsenic introduction to the system	56
4.5	Activity changes	59
Chapter 5	Conclusions	65
Bibliography		67

List of Tables

<u>Table</u>		<u>Page</u>
3.1	Criterion DN 200hydrotreating catalyst composition	23
4.1	Nitrogen and sulphur content comparison between night and day sample	47
4.2	Different reaction order equation and their R-square values	54
4.3	Arsenic content at different points of the cross section of the catalyst pellet	57
4.4	Arsenic content in the top, middle and bottom of the catalyst bed	59
4.5	Comparison between Ea values before and after arsenic intake	60
4.6	Arsenic effects on sulphur and nitrogen conversion at different LHSV	62
4.7	Comparison between arsenic adsorption and dissociation energies at different edges.	64

List of Figures

<u>Figure</u>		<u>Page</u>
2.1	Some organosulfur compounds on petroleum	5
2.2	Reaction pathways in the HDS of Dibenzothiophenes	6
2.3	Some nitrogen compounds present in petroleum distillates	7
2.4	Hydrodenitrogenation of pyridine	7
2.5	Scheme for the HDM pathways proposed for some Ni-Porphyrins	11
3.1	Process flow diagram for the hydroprocessing system	26
3.2	Control panel of the equipment control system	28
3.3	Schematics of the reactor loading	33
3.4	Schematic of the purging system	37
4.1	a. C curve for the trickle bed reactor using the scrubber as sample collector without water. b. Perfect pulse input representation compared to the pulse response.	43
4.2	C curve using the scrubber with water as sample collector	44
4.3	Peclet Number vs Superficial Velocity	45

4.4	Temperature profile along the catalyst bed with different shields	48
4.5	Differences in configuration between the reactor with aluminum jacket and with copper jacket	49
4.6	LHSV effects on HDS and HDN at 315°C, 30 bars and hydrogen/oil ratio of 500 ml/ml	51
4.7	Temperature effects on HDS and HDN at 2 h ⁻¹ , 3 MPa and hydrogen/oil ratio of 500 ml/ml	52
4.8	Fit of experimental data to the power law model for sulphur removal	54
4.9	Fit of experimental data to the power law model for nitrogen removal	55
4.10	Arrhenius plot for HDS and HDN	56
4.11	SEM/EDX picture of the cross section of the catalyst pellet	57
4.12	Sulphur conversion as a function of time on stream	61
4.13	Nitrogen conversion as a function of time on stream	62

Nomenclature

\AA	Angstrom
a_w	Ratio of wetted external area to total external area
$^{\circ}\text{C}$	Celsius Degree
C_f	Feed concentration
C_p	Product concentration
d_p	Particle diameter
E_a	Activation energy of reaction
g	Grams
g	Gravitational acceleration
G_L	Mass flow rate per unit area
HDA	Hydrodearomatization
HDM	Hydrodemetallation
HDN	Hydrodenitrogenation
HDS	Hydrodesulphuration
h^{-1}	1/hour
k	Rate constant
k_o	Arrhenious constant
Kj/mol	Kilojoules/mole
LHSV	Liquid hourly space velocity
mm	Millimeter
min	Minutes
MPa	Mega Pascal
n	Rate order

η	Effectiveness factor
N_f	Nitrogen concentration on the feed
N_{Eo}	Eotos number
N_{pe}	Peclet number
N_{we}	Weber number
$(N_{Ga})_L$	Galileo number of liquid
$(N_{Re})_L$	Reynolds number of liquid
$(N'_{Re})_L$	Modified Reynolds number of liquid
Ln	Natural logarithm
ppm	Part per million
R	Ideal gas constant
SEM	Scanning electron microscopy
S_f	Sulfur concentration on the feed
S_p	Sulfur concentration on the product
T	Temperature
W%	Weight percent
μl	Microliter
β_f	Dinamic hold up
β_r	Static hold up
β_t	Total hold up
σ_C	Critical surface tension
σ_L	Liquid surface tension
ρ_L	Fluid density

μ_L	Fluid viscosity
ν_L	Kinematic viscosity
v_{oL}	Superficial velocity
γ	Dependencies on viscosity, surface tension, density and particle size
E	Bed porosity
Z	Bed length

Chapter I

INTRODUCTION

The increasing demand for non-conventional oil sources, along with increasing environmental considerations and regulations, have resulted in the research and development of catalytic hydroprocesses to improve the quality of oil feeds by removing metals, and heteroatomic species such as sulfur and nitrogen from oil feedstocks. Heteroatomic species such as nitrogen and sulfur are the cause of environmental concerns because they produce SO_x and NO_x during combustion. Heteroatomic species and metals also cause concern in downstream processes because of catalyst poisoning and deactivation. Hydroprocessing consist of processing an oil feed at high hydrogen pressure and at relatively low temperature in the presence of a catalyst. The catalysts typically used during hydroprocessing are sulfided NiMo or CoMo supported on $\gamma\text{-Al}_2\text{O}_3$. Hydrodesulfurization and hydrodenitrogenation remove heteroatoms such as sulfur and nitrogen, producing H_2S and NH_3 . At the same time, hydrodemetallation processes metals cense to be deposited on the catalyst as sulfides, causing irreversible fouling and increasing the diffusional resistance of the reacting molecules. Carbonaceous deposits also called coke form in catalyst surface. Coke is believed to be primarily responsible for the initial aging of the catalyst, whereas deposition of metals continually deactivates the catalyst.

Therefore, metals eventually define the lifetime of the catalyst. Catalyst deactivation due to metals has a severe impact on the economics of hydroprocessing because it is irreversible and the catalyst must be replaced while a catalyst deactivated by coke can be regenerated and reused. There is a great wealth of information available about catalyst deactivation caused by coke and metals such as vanadium and nickel. Arsenic has also been recognized to have a dramatic influence on catalyst activity; however deactivation of hydroprocessing catalysts due to arsenic is a process that has not been studied to the same degree [2-5]

Naphtha hydrotreating catalyst deactivation is thought to be the result of arsenic poisoning of the active phase together with carbon deposition due to coking. However, the mechanism and extent of naphtha catalyst deactivation by arsenic is not known. Additionally, the deactivation kinetics and amount of arsenic the naphtha hydrotreating catalyst can tolerate before a significant reduction in activity occurs is a poorly understood phenomenon [2].

The principal objective of this research was the experimental study of naphtha hydrotreating catalyst deactivation due to arsenic compounds in order to validate previous molecular simulation studies. For this reason the development and installation of a bench scale trickle bed reactor system was necessary in order to perform the experimental tests and determine the

influence of process operating variables such as temperature and liquid hourly space velocity on the hydrodesulfuration and hydrodenitrogenation of light gas oil. Once the reactor system was established, experiments to determine the effects of arsenic on the hydrodesulfuration and hydrodenitrogenation of a light oil feed were performed. The composition of the spent catalysts was also investigated to determine the arsenic distribution within the catalyst pellet.

Ultimately, the results of this research project will help in the development of a control and optimization strategy to minimize the deactivation of hydrotreating catalysts.

Chapter II

LITERATURE REVIEW

2.1.1 Hydrotreating

Hydrotreating is a process that catalytically removes heteroatom impurities and metal compounds in crude oils. These impurities are usually organic compounds containing sulphur, nitrogen and metals that must be removed in order to control air pollution and poisoning of catalyst in downstream processes [6-10]. Hydrotreating involves the process reactions for the removal of S-compounds, N-compounds and M (metal) –compounds and are classified as hydrodesulfuration (HDS), hydrodenitrogenation (HDN) and hydrodemetallization (HDM) respectively.

During the hydrotreating process the oil feed is mixed with hydrogen before or after it is preheated and directed to a reactor which usually operates in a down-flow mode. Temperatures normally are under 410°C to minimize cracking. The oil feed with the hydrogen enters at the top of the fixed bed reactor. In the presence of an active supported metal catalyst, the oil and the hydrogen react to produce hydrogen sulphide, ammonia and metal sulphides [11].

2.1.2 Hydrodesulphuration

The difficulty in removing sulphur compounds from a petroleum stream is related to the structure of the sulphur compound to be treated. Sulphur compounds such as thiophene (see Figure 2.1), which has the sulphur in a five membered aromatic ring structure are much less reactive than aliphatic sulphur and the reactivity decreases as the number of rings increases. However, for compounds with a structure of four or more rings, the reactivity tends to increase. This increase on reactivity occurs because of the different chemical pathways that exist for sulphur removal and the preferred pathway depends on the sulphur compound structure [11].

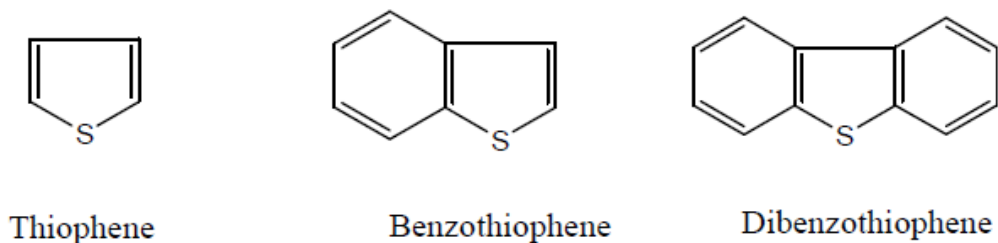


Figure 2.1 Some organosulfur compounds in petroleum (Gray, 1994)

The HDS of thiophenic compounds occur following two main pathways. Figure 2.2 shows a scheme of the two pathways for the HDS of dibenzothiophene. The first pathway, is direct hydrodesulphuration (following paths 3, 6 and 7 in the Figure 2.2) where the sulphur atom is removed from the structure and replaced by hydrogen without

hydrogenation of any other carbon-carbon double bonds. The second pathway is by hydrogenation of at least one aromatic ring adjacent to the sulphur containing ring before the sulphur atom can be removed (following paths 1, 2 and 4 in the Figure 2.2). After sulphur removal, aromatic rings can also be hydrogenated [12].

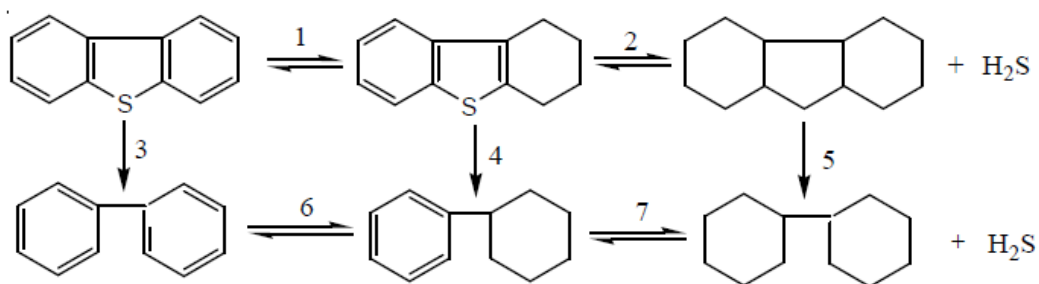


Figure 2.2 Reaction pathways in the HDS of dibenzothiophenes (Whitehurst et.al.,1998)

2.1.3 Hydrodenitrogenation

Nitrogen is mainly present as heterocyclic compounds, which occurs when the nitrogen atom is part of an aromatic ring structure [13]. The heterocyclic compounds are present in two forms: the basic and non-basic heterocyclic compounds (see Figure 2.3). Generally, basic nitrogen species contain a six-ringed structure while the non-basic compounds contain at least one five-ringed member [12].

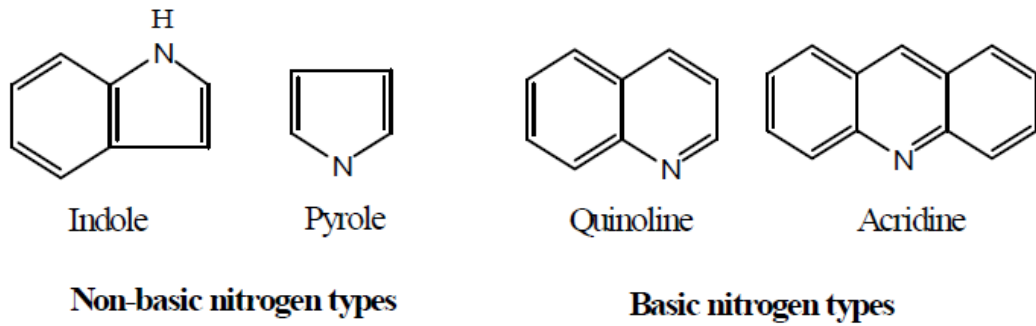


Figure 2.3 Some nitrogen compounds present in petroleum distillates (Gray, 1994)

HDN of heterocyclic compounds follow a hydrogenation pathway for nitrogen extraction. During the hydrogenation, heterocyclic rings must be saturated with hydrogen; also, other rings attached could also be hydrogenated. This step reduces the energy of the CN bond in the ring facilitating the CN bond cleavage. Figure 2.4 illustrates the HDN reaction pathway in pyridine.

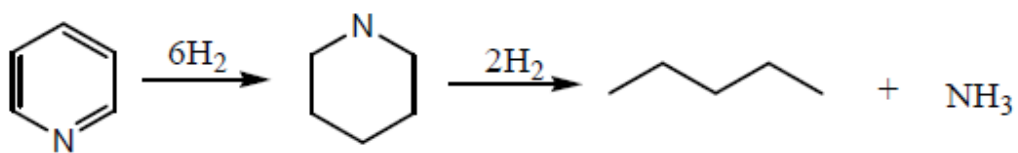


Figure 2.4 Hydrodenitrogenation (HDN) of Pyridine [12]

High hydrogen partial pressures are usually used in the industry to force equilibrium towards the products thus, making HDN irreversible.

2.1.4 Hydrodemetallation

Petroleum feedstocks contain trace metals in the form of organometallic compounds. The important and most studied metals found in oil feeds are iron, nickel and vanadium (these are organically bound and can not be removed by standard washing techniques). The arsenic content in some feeds is often overlooked, although it requires attention because of its adverse effects on catalysts. Additionally, arsine (one of the possible hydroprocessing products) is one of the most toxic species listed by health authorities [14]. During HDM metal byproducts deposit as insoluble sulphides on the catalyst surface. For this reason, as metals accumulate the lifetime of the catalyst is seriously affected as well as the production of desired products declines. Thus, HDM processes must be designed to prevent severe deactivation of the catalyst since deposited metal sulphides would fill its pores or sites.

It is generally accepted that there are two main types of metal compounds in petroleum feeds: metal porphyrins and non porphyrins metal species; these differ in properties such as molecular weight and structure. The focus of scientific research towards HDM has been directed to porphyrins. Due to the detrimental effect of the deposited vanadium in the catalyst, more attention has been dedicated to the V- containing porphyrins than to nickel containing porphyrins [14]. Compared with the deactivation due to nickel

and vanadium metals, deactivation of hydrotreating catalyst by arsenic is less frequently studied. Several recent studies have reported the deactivation of Ni/Al₂O₃ catalysts using an artificially arsenic concentrated feed stream. The interaction between the catalyst surface and the formation of metal deposits are discussed later in the catalyst deactivation section.

Figure 2.5 shows a scheme for the HDM pathways proposed for some Ni-porphyrins.

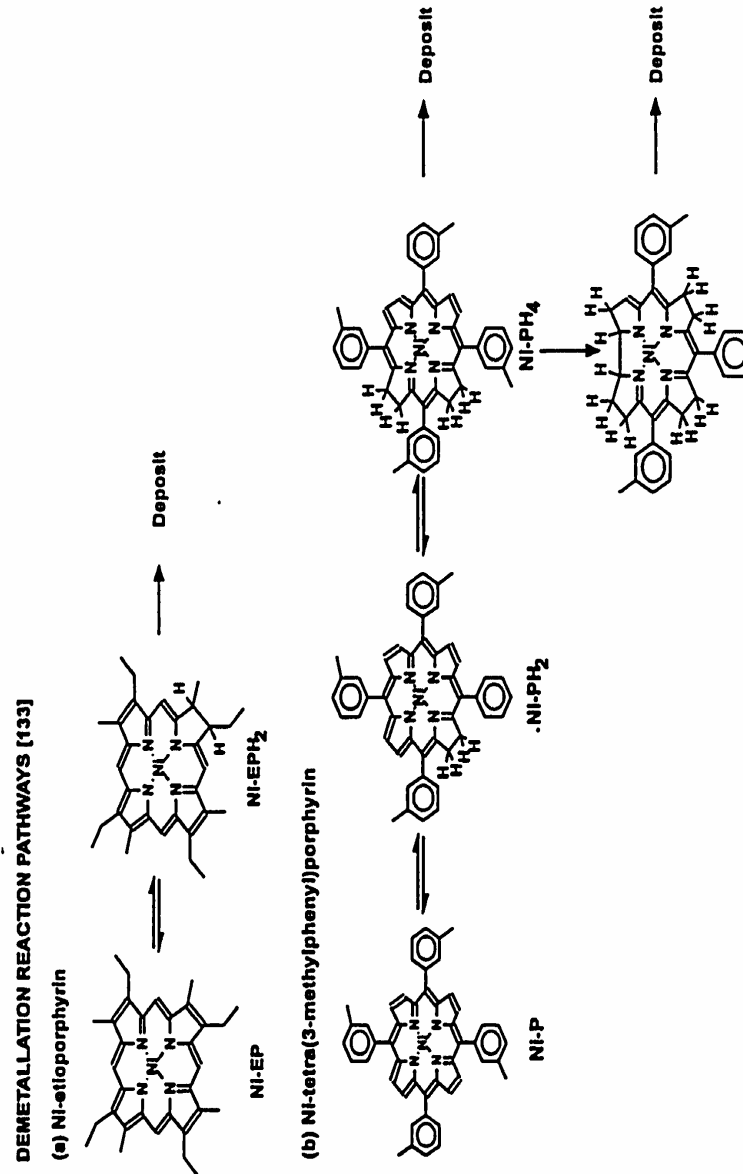


Figure 2.5 Scheme for the HDM pathways of some Ni porphyrin (Kwak, et al. 1994)

2.2 Hydrotreating Catalysts

Hydrotreating catalysts generally contain 1-8% w% and 3-20% of a group VIII and VI metal oxides usually supported on γ -Al₂O₃ characterized for having a high surface area [13]. The catalyst is selected depending on the nitrogen and sulphur content of the petroleum feedstock. Sulfided NiMo or CoMo on γ -Al₂O₃ is typically used. Conventional CoMo supported on alumina catalyst contains 3% CoO, 14% MoO₃ and this is well recognized for being one of the most used HDS catalyst due to its high activity and selectivity. NiMo catalysts usually contain approximately 3% Ni and around 10-16% of Mo and these are well known for their hydrogenation activity and have been used in HDN of petroleum feedstocks[1].

Usually hydrogenation catalysts are used in the reduced and sulfided form; practical experience supports the catalyst presulfiding prior operation with the petroleum feedstock [14]. These catalysts exist as a sulfides containing one Ni or Co atom in combination with two Mo or W atoms, on a solid support (alumina or silica alumina) (Whitehurst et.al., 1998). Sulfiding is done by contacting gaseous hydrogen sulfide or a low-boiling liquid phase sulfur- containing compound with the catalyst in the presence of hydrogen. Sulfiding temperatures are within the range of 180-350°C and at pressures greater than 1.0MPa (Speight, 2000). For real feed operations, the commonly used temperatures are 193°C and 343°C at 9.0MPa. Absi-Halabi

et al. demonstrated that presulfiding increased the rate of HDM and HDA (hydrodearomatization), also that in situ presulfiding using a sulphur containing oil was less efficient than the ex-situ presulfiding method.

In order to have an optimum catalyst, physical properties such as surface area, pore radius and pore volume should be aligned with the feedstock characteristics. A general classification of catalysts according to the median pore diameter will be: small pore catalyst with a median pore diameter less than 100Å, intermediate pore catalyst with pore diameters between 100-150Å and large pore catalyst with pore diameters above 150Å [1]. A small- intermediate pore volume catalyst with proportionate high surface area is very active for HDS because of the efficient dispersion of active metals in the pores [14]. However, in the case of high molecular weight feeds (heavy feeds) these pores are blocked and deactivated by pore mouth plugging. On the other hand, catalysts with large pore volume and small surface area are less active but more resistant to deactivation by pore mouth plugging, making them a good selection for HDM and HDA. Results [14] have shown opposite trends in the relationship between activity and average pore diameter for HDS and HDM. Because of restrictive diffusion, low conversion was found for HDM with a catalyst possessing an intermediate to small average pore diameter. Conversely, decreasing the average pore diameter favoured the HDS activity.

Another parameter that affects the catalyst effectiveness is the shape and size of catalyst particles. Large catalyst particles offer low pressure drop and less bed plugging in a fixed bed reactor. However, such large particles result in reduction of the effective surface area. Decreasing the particle size of a catalyst would improve its effectiveness; however, a small size catalyst will lose its activity at a faster rate due to coke and metal deposits. Also, these particles are susceptible to breakage and would cause large pressure drops in fixed bed reactors [14]. However, problems with the mechanical strength of particles may be overcome by selecting the proper shape of particles.

2.2.1 Catalyst Deactivation

The main shortcoming of hydroprocessing petroleum feedstocks has been the limited life of the catalyst. Deposits of coke and metal sulphides in the catalyst pores have been linked to an irreversible catalyst deactivation [15]. The most abundant and most studied metals found in petroleum feedstocks are vanadium and nickel which resides in asphaltic compounds called porphyrins. Reaction of these metals form metal-sulphide deposits that together with coke accumulate in the catalyst pores and results in constriction of pore mouth and ultimately plugging of the pores. A less frequently studied metallic element present in low-ppm or ppb levels in many crude oils is arsenic (Stigter, et al., 2000). Under hydroprocessing

conditions, organic compounds of arsenic are very reactive. Thus, they are converted to arsine or decompose and adsorb into the catalyst surface where they may be converted to sulphides.

In comparison to coke formation, metal accumulation on catalysts proceeds much slower mainly because the inlet concentrations of the metals are significantly lower than carbonaceous coke precursors [11]. The accumulation of metals, however, can be even greater than coke accumulation over the entire catalyst life

Nickel and vanadium accumulation on NiMoS catalysts has been widely studied while the mechanism of arsenic accumulation and catalyst deactivation is a poorly understood phenomenon. The significance of arsenic deactivation can be evidenced by the fact arsenic sorbent material is often installed in a guard reactor in order to prevent arsenic from coming into contact with the NiMoS hydrotreating catalyst [2]. Current arsenic removal sorbents are comprised of Ni-Mo supported on Al_2O_3 [3], and effectively remove arsenic from naphtha by sacrificing the nickel to form NiAs. However, arsenic can remain in the guard reactor effluent either through incomplete sequestering of the arsenic in the guard reactor or by leaching of arsenic from the sorbent material. The effect of the residual arsenic can be pronounced with the measurable accumulation of arsenic in

the top bed of the naphtha hydrotreater within several months of operation [2]. In order to prevent the deactivation of the NiMoS hydrotreating catalyst, additional insight into the mechanisms and energetics of arsenic deactivation is required.

Several recent studies have reported the deactivation of Ni-Al₂O₃ catalysts using an artificially arsenic concentrated feed stream. These studies have demonstrated that on a Ni-Al₂O₃ catalyst deactivation proceeds via a stepwise process by the initial formation of arsenic adatoms, the diffusion of these adatoms into the supported nickel particles to form intermetallic Ni_xAs_y phases, and the final formation of crystalline NiAs [10]. Additionally, studies using nickel reforming catalysts have also proposed the formation of Ni₅As₂ and NiAs nickeline alloy phases [5]. Considering the significantly lower amount of nickel in the NiMoS hydrotreating catalyst and the unique structure of the bimetallic NiMoS phase, the deactivation mechanism of NiMoS is expected to be considerably different than the mechanism for highly loaded Ni-Al₂O₃ catalysts [2].

Information regarding the mechanism and chemical state of arsenic after deposition on a NiMoS naphtha hydrotreating catalyst is scarce. Yang et al [2] studied arsenic poisoning of NiMoS hydrotreating catalysts using density-functional theory (DFT) calculations. In this research, the incorporation of arsenic into NiMoS by chemical adsorption and

dissociation of organoarsenic molecules (AsH_3 , $(\text{CH}_3)_3\text{As}$, $(\text{C}_2\text{H}_5)_3\text{As}$, and $(\text{C}_6\text{H}_5)_3\text{As}$) and the substitution of Ni and S atoms by arsenic on both fully promoted Ni(100)Mo- and Ni(100)S-edge surfaces were investigated. Results show that the adsorption of organoarsenic compounds is energetically favored on both metal and sulphur edge surfaces and there is a correlation between the absorptivity of the arsenic compounds and their electronic structure. After the organoarsenic molecules have adsorbed on the edge surfaces, dissociation on a Ni (100) S-edge surface is energetically favored. Arsenic may substitute Ni atoms on both Ni (100) Mo-edge and Ni (100) S-edge surfaces. However, the substitution of S atoms by arsenic may only occur on the Ni (100) S-edge surface.

2.3 Trickle Bed Reactor Hydrodynamics

The movement of the liquid and gas through the catalysts bed inside the reactor is called hydrodynamics. The hydrodynamics in trickle bed reactors is characterized by a number of parameters that will be discussed in the following section. The prediction of the performance and the scale up of this kind of reactors is a difficult problem to deal with because the reactors performance depends on complex hydrodynamics phenomena that influences the mass transfer processes occurring in the multiphase system [16].

2.3.1 Liquid Hold Up

The liquid phase hold up is expressed as the volume of liquid present per volume of empty reactor.

The liquid hold up in the reactor is subdivided into external hold up which is the liquid contained in the void fraction of the bed between the catalyst particles and the internal hold up that is related to the liquid inside of the catalyst pores.

The external hold up is divided in static and dynamic hold up. The static hold up is the liquid that remains in the bed after it has been drained. The simplest definition for the dynamic hold up is the difference between the total hold up and the static hold up. There are many correlations proposed in a number of studies for diverse hold ups.

The Eötvös number (N_{Eo}) is a nondimensional parameter correlated to the static hold up:

$$N_{Eo} = \left(\frac{\rho_L g d_p^2}{\sigma_L} \right) \quad (2.1)$$

This expression indicates the ratio of gravity to surface forces, where: ρ_L is the fluid density, g is the gravitational acceleration, d_p is the nominal

particle diameter and σ_L is the liquid surface tension. Satterfield et al., proposed the following correlation for the total hold up:

$$\beta_t = \beta_r + \beta_f = a(N_{Re})_L^{1/3} (N_{Ga})_L^{-1/3} \quad (2.2)$$

Here β_t is the total hold up, β_r is the static hold up, β_f is the dynamic

hold up, a is a proportionality constant, $(N_{Re})_L = \frac{G_L d_p}{\mu_L}$ where G_L is the

mass flow per unit area, μ_L is the viscosity and $(N_{Ga})_L = \frac{d_p^3 g \rho_L^2}{\mu_L^2}$. Other

hold up correlations that we can mention are; Midoux et al. [17] gave a

correlation for the total hold up for nonfoaming systems, Larkin et al. [17]

proposed a correlation for the dynamic hold up and Baldi and Gianetto [16]

also worked in a correlation for the dynamic hold up but for low interaction

regime. From this short review, it is noticeable that a large amount of data

for dynamic and total hold up is reported in the literature. Although there

are some discrepancies between correlations, the general behaviour

indicates that increasing liquid velocity will increase liquid hold up and that

increases in particle size appears to decrease the liquid hold up [18].

2.3.2 Catalyst Wetting

The hydroprocessing reactions occur normally in the liquid film around the

catalyst particles in the majority of the trickle bed reactors. For this reason,

it is very important for all the catalysts in the bed to be wetted by the liquid in order to use all the active sites in the catalyst in an effective way. The effectiveness of the catalyst wetting also relies on factors as the liquid hold up and the proper liquid distribution. Many studies (Mears [19], Paraskos et. Al. [20], Montagna [21] and Shah [18]) have demonstrated that ineffective catalyst wetting can cause the reactor performance to become dependent on the liquid velocity. In commercial reactors it is assumed that all the catalyst particles are wetted by the liquid but in a bench scale, where the flow rates are smaller, some particles are without a liquid film on their surface. These researchers used the correlation of Puranik and Vogelpohl [22] for introducing the catalyst wetting factor in their calculations:

$$aw = 1.05(N_{Re})_L^{0.047} (N_{We})_L^{0.135} \left(\frac{\sigma_c}{\sigma_L} \right) \quad (2.3)$$

Where $(N_{We})_L = \left(\frac{G_L^2 d_p}{\sigma_L \rho_L} \right)$, σ_L is the liquid surface tension and σ_c is the critical surface tension for contact. Introducing the Puranik and Vogelpohl wetting factor in the overall reaction rate the equation will be:

$$\ln \left(\frac{C_o}{C_{out}} \right) = - \frac{Z^{0.32} d_p^{0.18} \left(\frac{\sigma_c}{\sigma_L} \right)^{0.21} \eta}{LHSV^{0.6} v_L^{0.05}} \quad (2.4)$$

Here, Z is the bed length; η is the effectiveness factor and ν_L the kinematic viscosity. The correlation of Onda et al. should be used in cases where there are high liquid rates.

$$aw = 1 - \exp \left[-1.36 G_L^{0.05} (N_{We})_L^{0.2} \left(\frac{\sigma_c}{\sigma_L} \right)^{0.75} \right] \quad (2.5)$$

In this case the overall reaction equation will be:

$$\ln \left(\frac{C_o}{C_{out}} \right) = \frac{k(1-E)\eta}{LHSV} \left[1 - \exp \left\{ -\gamma Z^{0.4} LHSV^{0.4} \right\} \right] \quad (2.6)$$

Where, the factor γ represents the dependencies on viscosity, surface tension, density and particle size.

2.3.3 Axial Dispersion

Experimental results have shown that in trickle bed reactors significant axial mixing occurs. The Peclet number N_{pe} is the parameter by which the residence time distribution is described. There many correlations proposed. Michell and Furzer [23] correlated their data along with other researchers' data by the following relation:

$$(N_{Pe})_L = (N_{Re})_L^{0.70} (N_{Ga})_L^{-0.32} \quad (2.7)$$

Where $(N_{Pe})_L = \frac{v_L d_p}{D_L}$, $(N_{Re})_L = \frac{d_p \rho_L v_L}{\mu_L}$ and $(N_{Ga})_L = \frac{d_p^3 g \rho_L^2}{\mu_L^2}$. Here, v_L is

the interstitial liquid velocity and D_L the axial dispersion coefficient.

Furzer and Michell also correlated the Peclet number to the dynamic hold up by the relation:

$$(N'_{Pe})_L = 4.3 \left[\frac{(N'_{Re})_L}{\beta_f} \right]^{1/2} (N_{Ga})_L^{1/3} \quad (2.8)$$

In this relation the Reynolds number was defined in terms of superficial liquid velocity $(N'_{Re})_L = \frac{\rho_L v_L}{a_s \mu_L \beta_t}$. However, the dependence of the Peclet number on the Galileo number is not reliable because all the data was obtained for air-water systems. The exception for the previous affirmation was the work done by Hochman and Effron [24] whom correlated their data by:

$$(N_{Pe})_L = 0.042 (N_{Re})_L^{0.5} \quad (2.9)$$

Here, $(N_{Re})_L = \frac{v_{OL} \rho_L d_p}{\mu_L (1-E)}$ where v_{OL} is the superficial velocity and E is the

bed porosity. This equation is recommended for hydrocarbon systems [18].

Chapter III

MATERIALS AND METHODS

3.1 Materials and Chemicals

Light gas oil from plant #18 Syncrude, Canada was used as a feed to carry out the studies. This feed was used as supplied for kinetics experiments and doped with triphenylarsine from Sigma-Aldrich, Canada for the study of arsenic effects on the catalyst with an arsenic concentration on the feed of 100ppm.

Prior to experiments, the reactor saturation was done using a solution of 300 ppm of triphenylarsine in 1-methylnaphthalene, 95% reagent grade from Sigma-Aldrich Canada, LTD.

The reactor was loaded with silicon carbide of 16, 46, 80 mesh from Sigma-Aldrich Canada, LTD, in order to support the catalyst bed and as a diluent of the catalyst bed. The hydrotreating catalyst selected for this study was Criterion DN-200, its specific composition is listed in Table 3.1. This catalyst was presulfided and provided by Syncrude, Canada.

Solvents used as diluent for samples analysis, for cleaning materials used for feed preparation, sample collection, sample analysis and for flushing the reactor after reaction were provided by Fisher Scientific.

For sample analysis, dibenzothiophene 98% and indole 99% from Sigma-Aldrich Canada, LTD, were used as standards in order to built the calibration curve needed for sulphur and nitrogen detection using the Antek 9000 (sulphur and nitrogen analyzer).

Table 3.1 Criterion DN 200 Hydrotreating Catalyst Composition

COMPONENT	CHEMICAL FORMULA	CONCENTRATION
Aluminum oxide	Al_2O_3	67-77%
Molybdenum oxide	MoO_3	12-19%
Phosphorus pentoxide	P_2O_5	1-4%
Nickel oxide	NiO	10-14%

3.2 Experimental Equipment

In order to perform the experimental studies on the effect of arsenic on the deactivation of hydrotreating catalyst a micro trickle-bed reactor was used. The micro trickle-bed reactor system used in this study consisted of a liquid feed section; a gas feed section, a trickle-bed reactor and a liquid sample recollection section. The total system was designed for a simultaneous gas-liquid down flow operating mode where the hydrogen and the liquid feed were introduced on the top of the reactor. This operating mode is similar to

commercial trickle-bed reactors used for hydrodenitrogenation and hydrodesulfuration. An advantage of the down-flow mode is that higher liquids flow rates are possible without flooding [25]. The product liquid and gas were passed through a water condenser prior to collection. The liquid samples were withdrawn from a collector at the bottom of the condenser and the gas was directed to a back pressure regulating valve. The process flow diagram for the hydroprocessing system is presented in Figure 3.1.

3.2.1 Hydrogen Feed Line

Hydrogen feed was provided by Praxair gases in cylinders with an initial pressure of 13,8 MPa; the hydrogen had a purity of 99.99%. A regulator was used to control the pressure of the cylinder up to around 3 MPa (0.15 MPa above of the required system pressure). When the cylinder pressure was below 3.5 MPa the hydrogen cylinder was changed. After a cylinder exchange, the line was purged of air. The hydrogen flow was controlled in the inlet by a check valve (denoted as V3 in Figure 3.1) followed by a solenoid valve (N.O.) and a pressure indicator (denoted as PI in Figure 3.1) just before the mass flow controller (Brooks model 5850S/BC, denoted as MFC1 in Figure 3.1). The mass flow controller was calibrated at the following conditions: Maximum flow 1000ml/min, inlet pressure 5.5 MPa, outlet pressure 5.2 MPa, temp 20°C, gas, hydrogen. After the flow

controller the hydrogen feed line had two check valves and two ball valves (denoted as V4 and V5 in Figure 3.1) followed by a T connection where the hydrogen line is intersected by the liquid feed line.

3.2.2 Liquid Feed Line

From a 500 ml glass feed bottle, liquid feedstock was pumped into the reactor by a Gilson 307 programmable reciprocating pump. This pump had a single piston and a pressure feedback. The working range was as follows: flow rate 0.010-5 ml/min, pressure 0-4 MPa, temperature 0-40°C. After the pump, one check valve and a ball valve (denoted as V18 in Figure 3.1) was installed before the T connection where this line intersected the hydrogen feed line.

3.2.3 Reactor

The reactor was custom made at the University of Alberta machine shop. Stainless steel 19 mm tubing (Swagelock) was used for the reactor construction. The inner diameter was 17.4 mm and the wall thickness was 1.6 mm. The reactor length was approximately 500 mm without the gaskets used for sealing. The sealing gaskets of the reactor are the reduction for the 6.35 mm tubing used for all the lines of the system. At the top of the reactor two needle valves were installed; one for reactor isolation from upstream lines and the other for pressure relief (denoted as V8 and V9 in

Figure 3.1). At the bottom of the reactor a needle valve was located for reactor isolation (denoted as V10 in Figure 3.1). The trickle-bed reactor was operated in a continuous concurrent down flow mode and heated by a single zone electric Lindberg tube furnace (HTF55322C 1200 °C furnace), configured in a vertical position.

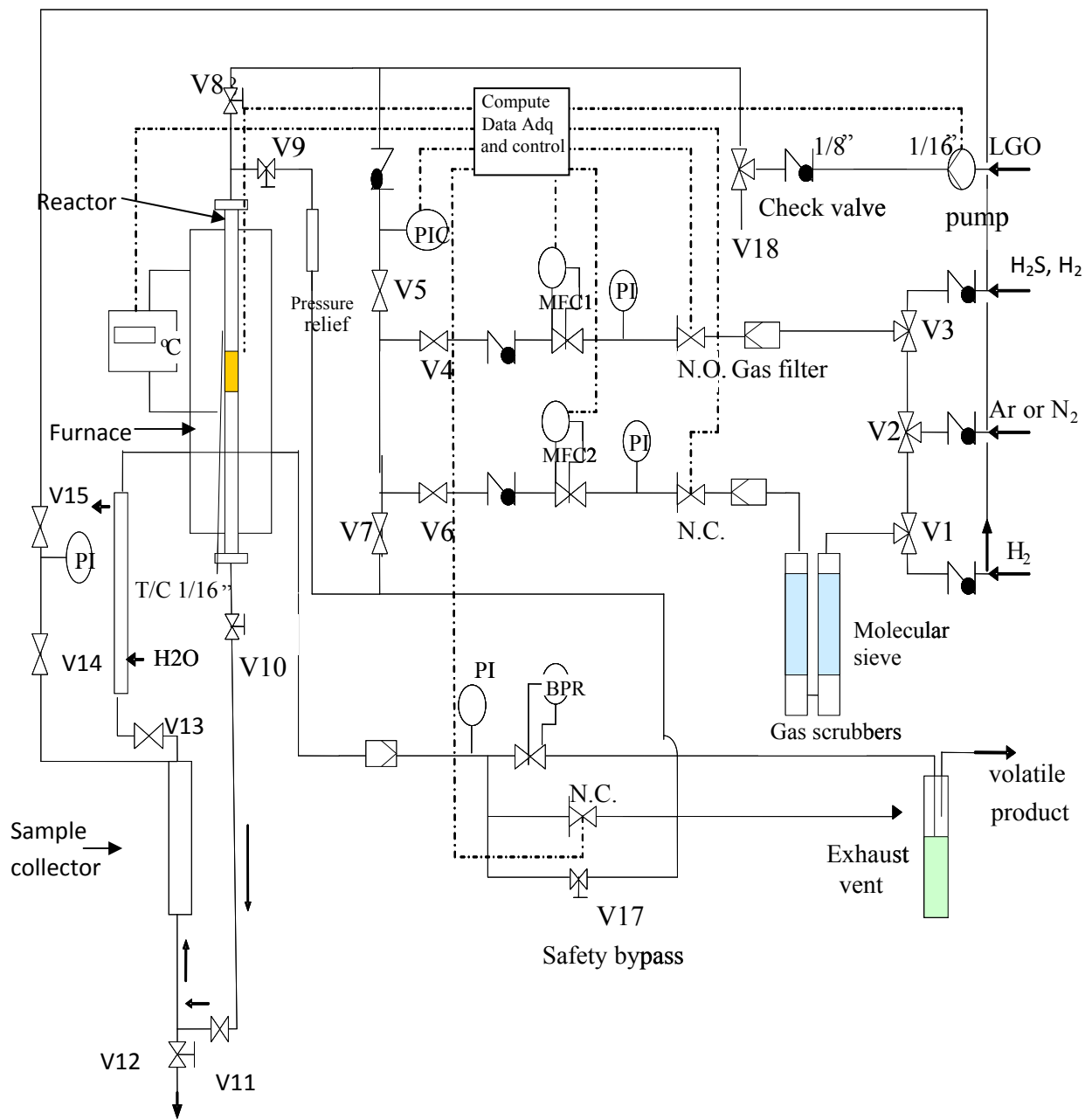


Figure 3.1 Process flow diagram for the hydroprocessing system

The temperature in the furnace was controlled by an independent digital temperature control module (Lindberg/Blue M CC58114). The temperature along the reactor was monitored by a movable thermocouple connected to the control system. Figure 3.2 shows the control panel of the equipment control system. This panel monitored the temperature of the reactor given by the movable thermocouple from the top, middle or bottom of the catalyst bed which was positioned in the middle of the reactor and furnace.

Initially, significant differences in temperature between the thermocouple and the furnace digital temperature control and between the top and the bottom of the catalyst bed were observed. For this reason, a copper coating was designed in order to minimize temperature differences.

The efficiency of this procedure led us to develop an aluminum shield that was used to prevent temperature fluctuations and to maintain an isothermal temperature profile in the catalyst bed. The aluminum shield was designed with an entry port on one side in order to introduce the thermocouple and monitor the temperature of the reactor along the catalyst bed.

3.2.4 Pressure Control System

The system pressure was maintained, monitored and controlled by a back pressure regulator valve, a bourdon tube pressure gauge with electrical contact device and various pressure indicator gauges along the system.

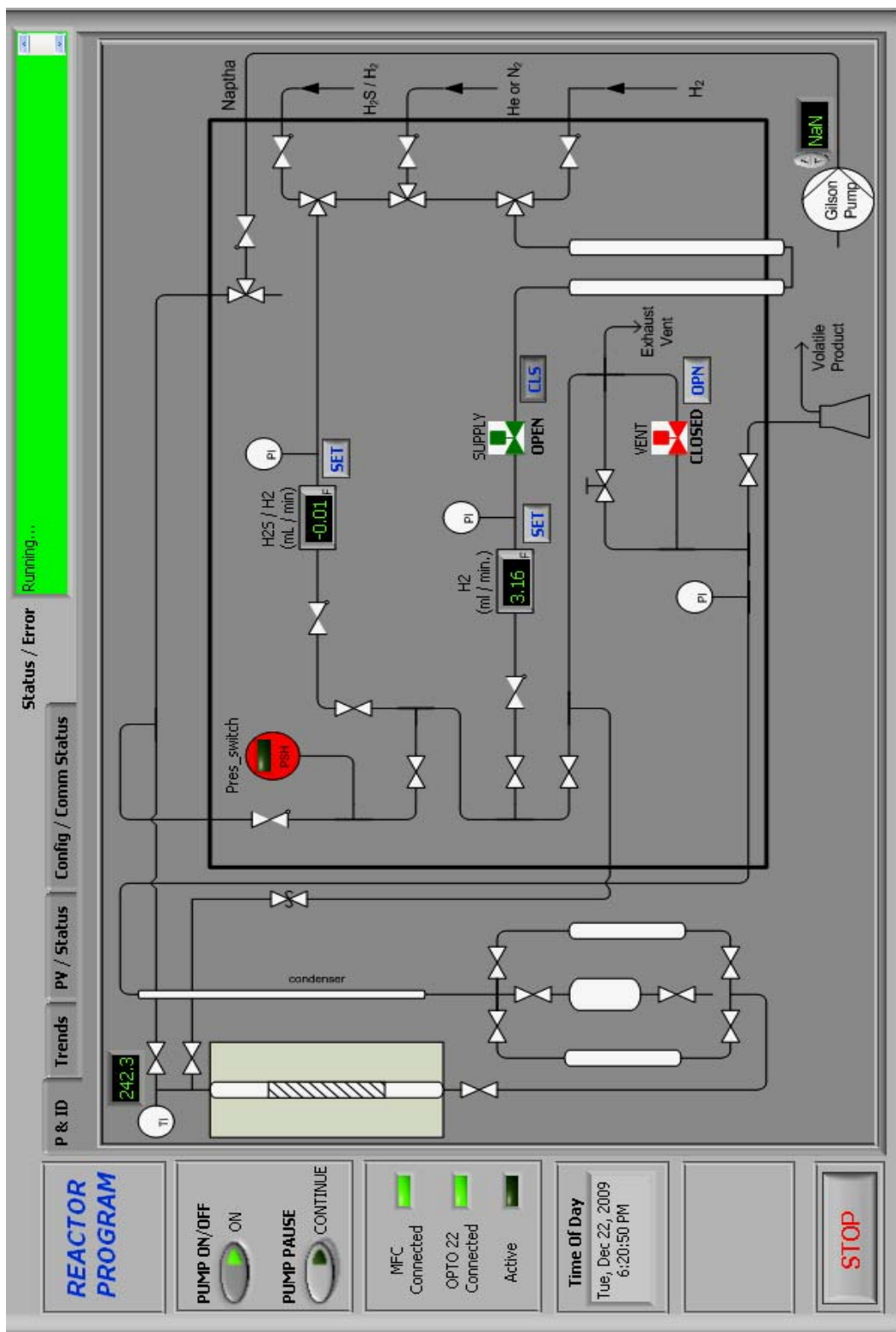


Figure 3.2 Control panel of the equipment control system

The back pressure regulator (BPR in Figure 3.1) was located in the product line after the condenser. This valve controlled the system pressure by controlling the flow of product gas coming from the condenser. The regulator allowed the gas to exit from the system when the teflon diaphragm was deflected due to a value of pressure above of the set value in the valve.

The bourdon tube pressure gauge (denoted as PIC in Figure 3.1) was located in the hydrogen feed line just before the intersection with the liquid feed line. The pressure gauge had a pre-selectable minimum and maximum pressure value, if the pressure went above or below the desired values; the control system automatically shut down the pump and closed the solenoid valve in the hydrogen line feed.

Additionally, pressure gauges (denoted as PI in Figure 3.1) were located in the hydrogen feed line before the hydrogen mass flow controller, in the H₂S/H₂ feed line before the mass flow controller, in the pressure compensation system located in the sampling line and before the back pressure regulator.

3.2.5 Argon, Nitrogen, Hydrogen Sulphide and Hydrogen Feed Line

After reactions were completed, argon was used to purge the feed lines. Argon feed was provided by Praxair gases with an initial pressure of

13.8MPa. A regulator was used to control the pressure of the cylinder up to around 0.6 MPa. The argon flow was controlled using a check valve followed by a solenoid valve (N.O) and a pressure indicator (PI) before the (Brooks) mass flow controller (MFC1) calibrated as follows: maximum flow of 25 ml/min, inlet pressure 5.5 MPa, outlet pressure 5.2 MPa, temperature 20°C. After the flow controller, this line also had one check valve and one ball valve followed by a T connection for intersecting the hydrogen feed line before the last ball valve, preceding the Bourdon pressure gauge (PIC).

3.2.6 Liquid Product Sampling Line

After the tubular reactor, a needle valve (denoted as V10 in Figure 3.1) was used to control the flow to the separator cylinder. This cylinder (260 ml) had a top ball valve (N.O during reaction) and a bottom needle valve to allow the collection of the liquid product sample. The collector was connected from the top with a condenser. Condensed vapours were collected in an Erlenmeyer flask (500ml) and the gas was directed to the back pressure regulator.

After initial testing, a pressure compensation system was added to the separator cylinder. This system consisted of a line coming from the hydrogen inlet connected to the separator cylinder through a metering valve

and a ball valve. This pressure compensation line was fitted with a pressure indicator.

The NH_3 and H_2S in the exit gases were absorbed in a 1 molar solution of NaOH contained in a 500 ml vessel connected to the exit of the back pressure regulator through a flexi tube.

3.3 Experimental Procedure

3.3.1 Reactor Loading

The reactor was loaded following the schematics shown in Figure 3.3. The reactor length (50 cm) was divided in three zones: the inlet zone (preheating), the catalyst bed and the exit zone. Packing of the reactor was performed in reversed order.

Exit zone:

Glass wool and a small metal support were introduced for beginning the reactor loading. In the bottom of the reactor were 35 ml of glass beads followed by 6 ml of 16 mesh, 3 ml of 46 mesh and 2 ml of 80 mesh silica carbide. The previous components were in the exit zone of the reactor and were the support for the catalyst bed.

Reaction Zone:

Three grams of catalyst were divided in 12 identical parts (0.25 g), with each part diluted with 0.5 ml of 80 mesh silica carbide. After loading 4 diluted parts of catalyst, glass wool was used to separate the catalyst bed into three parts: bottom, middle and top of the catalyst bed.

Inlet Zone:

After the loading of the catalyst bed, the inlet zone was loaded with 2 ml of 80 mesh silica carbide, 2ml of 46 mesh silica carbide, 6 ml of 16 mesh silica carbide and finally 26 ml of glass beads.

Stainless steel gaskets were used to seal the unit. Finally, the reactor body was connected to the hydrotreating system. A schematic of the reactor loading is shown in Figure 3.3.

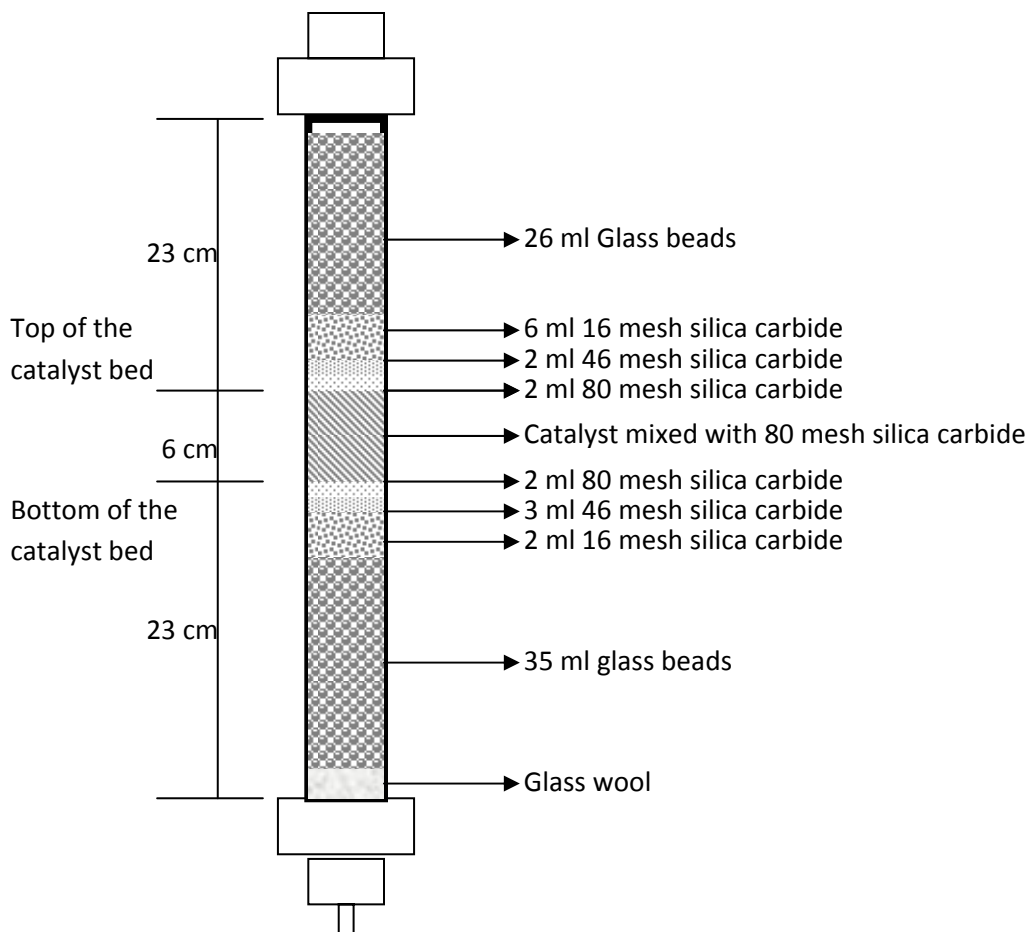


Figure 3.3 Schematic of the reactor loading.

3.3.2 Pressure Leak Tests

The hydrotreating system was pressure tested prior to any experimental procedure in order to detect and prevent hydrogen leaks. The unit was separated in three sections and each section was checked independently. The first isolated section was from the hydrogen inlet to the valve at the bottom of the reactor (denoted as V10 in Figure 3.1). Hydrogen was fed by opening the solenoid valve in the inlet at a pressure of 3.1 MPa. The valve

and the cylinder were closed when a pressure of 3 MPa was reached. After an 8-hour period, if no loss of pressure was detected, the valve in the top of the separator cylinder (denoted as V13 in Figure 3.1) was closed and the valve at the bottom of the reactor opened (denoted as V11 in Figure 3.1). Hydrogen was fed to the unit until the 3 MPa pressure was reached again. For this section, the unit was monitored for leaks for a period of 16 hours. If there were no significant leaks, the valve at the top of the collector (denoted as V13 in Figure 3.1) was opened allowing free feed of hydrogen until a pressure of 3 MPa was achieved in the system. Maintaining the hydrogen feed line open, the back pressure regulator was slowly opened until small bubbles are visible in the outlet vessel connected to the back pressure regulator.

If significant pressure drop was detected in any section that line was monitored with a hydrogen leak detector on each of its parts (valves and connections) until the source of the leakage was found. Once the leakage was detected the unit was tested again with hydrogen pressure.

3.3.3 Reactor Startup, Experimental Operation and Shut Down

To determine the effects of operating variables such as liquid hourly space velocity and temperature over hydrodenitrogenation and hydrodesulfuration, studies with light gas oil feed with and without added

arsenic were performed. The effect of arsenic on product conversion and kinetics were determined.

After the pressure leakage test, 100 ml of 1 M sodium hydroxide solution were prepared for the system discharge.

Light Gas Oil, provided by Syncrude, Canada from plant # 18, was used during all stages of the experiments, including catalyst initial deactivation, operational variable effects and arsenic quantity effects. For the experiments with arsenic, triphenylarsine was doped in the light gas oil in order to achieve a feed with 100 ppm of arsenic.

After the feed preparation, pump priming was necessary for each start up. The procedure for priming began with the inlet tubing filter immersed in the feed vessel. Next a syringe was used to draw liquid from the prime valve which should be in the load position (open to the left side). After removing any air bubbles in the inlet, the valve was returned to the inject position (open to the right side). The prime button was pressed on the pump panel and the syringe was depressed until some liquid passed through the pump outlet. After this, the prime valve was returned to the run position, the syringe was removed and the stop button in the pump panel was pressed to stop the priming.

In order to begin running the liquid feed, a temperature of 200°C was required. To achieve this temperature the furnace was turned on and the temperature monitored until it reached 200°C.

At the beginning of each run a period of 4 days of stabilization and deactivation of the catalyst was necessary, within this period oil feed was pumped at 350°C, 3 MPa, and a LHSV of 1 h⁻¹.

The experiments were performed in two phases. The first phase included the variation of the liquid hourly space velocity and temperature (LHSV and T) using a light gas oil feed. LHSV and T were varied individually; the system pressure and one of the variables were constant while the other variable was manipulated within a reasonable range: for temperature a range of 315-345° C was used and for LHSV a range from 1-3 h⁻¹. Following these measurements, a period of catalyst exposure to a light gas oil feed with 100 ppm of arsenic added took place. During arsenic intake the LHSV was kept at 2 h⁻¹ with a temperature of 315°C for approximately 3-6 days. In this period samples were taken once a day. After the catalyst exposure to arsenic, the feed was changed to regular light gas oil (beginning of phase 2) and the effects of temperature and liquid hourly space velocity were measured as described above (phase 1). Experiments were performed at 315-345°C, 3MPa and liquid hourly space velocity of 1-3 h⁻¹. Hydrogen flow rate of 500ml/ml and 3 grams of the NiMo/γAl₂O₃ catalyst were

constant. Liquid samples were collected at 6-12 hours intervals depending on the flow rate established. After collection, the liquid product samples were purged in order to remove dissolved hydrogen sulphide that can interfere with the sample analysis. Each sample was placed in the purging system that consisted of a test tube with a side arm which was connected to an Erlenmeyer flask placed on ice that collected the purge (see Figure 3.4). The hydrogen sulphide and the ammonia were stripped from the sample with argon gas.

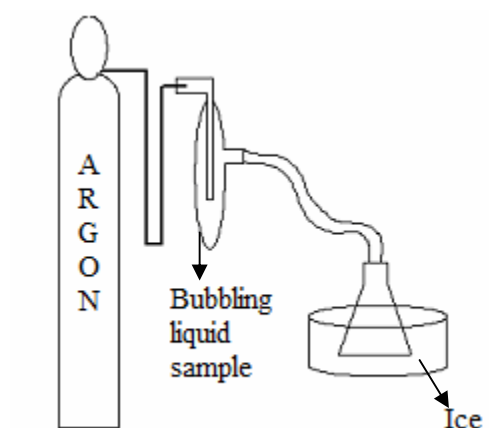


Figure 3.4 Schematic of the purging system.

Each experimental run took on average 21 days of continuous reaction. After the conclusion of each experimental study, the temperature in the furnace was decreased. When the temperature was approximately 100°C, the pump was stopped. When room temperature was reached, the pump was started using toluene as a feed for flushing the system. When the liquid exiting the reactor was clear, the pump was stopped and the gas feed

switched to argon. After a few of hours the gas was stopped and the pressure of the system slowly decreased. The reactor was disconnected, removed from the system and opened for removal of the catalyst.

3.3.4 Catalyst Sulfidation

The hydrotreating catalyst was received from Syncrude Canada, presulfided and precoked. The sulfidation was done at 193 and 343°C. The precoking was at 355°C with a light gas oil blend for seven days.

3.3.5 Reactor and System Saturation

Arsenic strongly adsorbs on steel surfaces. For this reason, all the exposed surfaces in the hydrotreating system, including reactor and stainless steel tubing parts, was fed with a solution of 1-metalnaphthalene and 300 ppm of triphenylarsine at a liquid hourly space velocity of 2 h⁻¹ with a reactor temperature of 300°C for a period of eight hours. During this time the saturation of exposed and wetted metal surfaces of the system with arsenic was expected.

3.3.6 Liquid Sample Analysis

Samples dilution was necessary prior to analysis. Liquid product samples were diluted 50% in toluene. Sulphur and nitrogen contents were measured using the fluorescence and chemiluminescence's method through the Antek 9000 equipment. A calibration curve was inputted into the equipment

software. For this calibration curve dibenzothiophene and indole dilutions were used as standards for sulphur and nitrogen content. After dilution, 10 μl of liquid samples were injected into the sample boat. Nitrogen and sulphur present in the sample are oxidized to NO_2 and SO_2 . The light released for the oxidation of nitrogen and the fluorescence emitted by the excited SO_2 are proportional to the nitrogen and sulphur present in the liquid sample.

Neutron activation analysis was used for arsenic measurement in the liquid samples. Samples were pipette to labeled plastic vial and sent to the Slow Poke Facility at the Pharmacy Department of the University of Alberta.

3.3.7 Catalyst Analysis

The active catalyst bed was divided in three parts for each run: the top, middle and bottom. After experiments with added arsenic, each catalyst part was analyzed for total arsenic content and for arsenic distribution inside the pellets. The total arsenic content in each part of the catalyst bed was measured through neutron activation analysis at the Slow Poke Facility at the University of Alberta. The Arsenic distribution through the pellet was studied by the Scanning Electron Microscopy facility located at the Chemical and Materials Engineering Department of the University of Alberta.

3.4 Safety measures

The safety concern in this research project was directed to the manipulation of arsenic, hydrogen and hydrogen sulfide.

Arsenic and arsenic compounds are classified as toxic and carcinogens. As a result of the possible occupational exposure incurred on this research project, the arsenic compound (triphenylarsine) selected for experimentations was one of the safest and the possibility of working with gaseous arsenic was rejected. Also, due to the concern of working with arsenic, the reactor operator was tested for a baseline of arsenic, keeping tracking of arsenic levels on the operator during the whole research project.

Hydrogen is well known for being highly flammable burning easily on air in a very wide range of concentration. For this reason, a procedure for checking leaks was done before every experiment having in addition a detector for combustible gases. It is noticeable that the whole reactor system was built in a fume hood in order to have an outstanding ventilation system and keep tracking that it was always working properly. Hydrogen cylinder was inside a safety cabin with proper ventilation.

Pre-sulphidation of the catalyst was done at Syncrude installations making unnecessary the contact of the catalyst and reactor system with any H₂S solution.

Additionally, along this section was mentioned the pressure control system that will shut down the reactor system if a dangerous condition (high pressures) exist.

Chapter IV

RESULTS AND DISCUSSIONS

4.1 Determination of the Residence Time Distribution in the Reactor System

The residence time distribution curves allowed the evaluation of the dynamic hold up of the fluid phases in the reactor [26]. In order to describe in a quantitative manner how much time fluid elements spent in the reactor the residence time distribution was determined experimentally by injecting 2 ml pulse of decane as the tracer with a flow rate of 1 ml/min. Simultaneously, toluene was running at 1 ml/min as the base feed. The tracer concentration, C , was measured in the effluent product as a function of time. RTD measurements were done with two sample collection configurations, one using a scrubber as a direct sample collector and another using a scrubber with water for sample collection. Figure 4.1 and Figure 4.2 show the curves resulting from the variation of the concentration with time. Figure 4.1.a shows the $C(t)$ curve for RTD experimental measurement using the scrubber as sample collector and Figure 4.1.b shows a comparison between the pulse input and the pulse response in this configuration. This $C(t)$ curve shows that for a pulse of 2 ml equivalent to 2 min, the reactor system takes 25 min for showing the tracer injection. This is consistent with the amount of mixing in a trickle reactor system.

Figure 4.2 represents the $C(t)$ curve using the scrubber with water for sample collection. It is remarkable that this curve has a long tail which according the literature is a result of flow maldistribution [18]. In this particular study the product sample was flowing through the water at the scrubber, making the sample collection a long process.

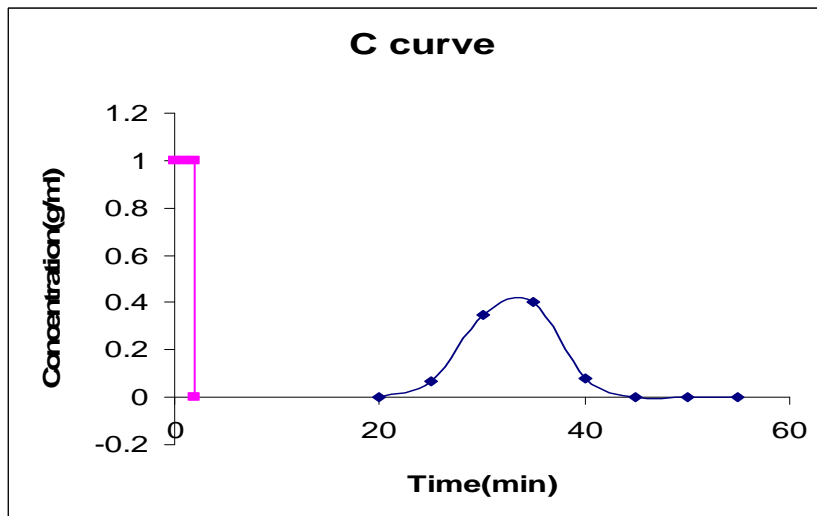
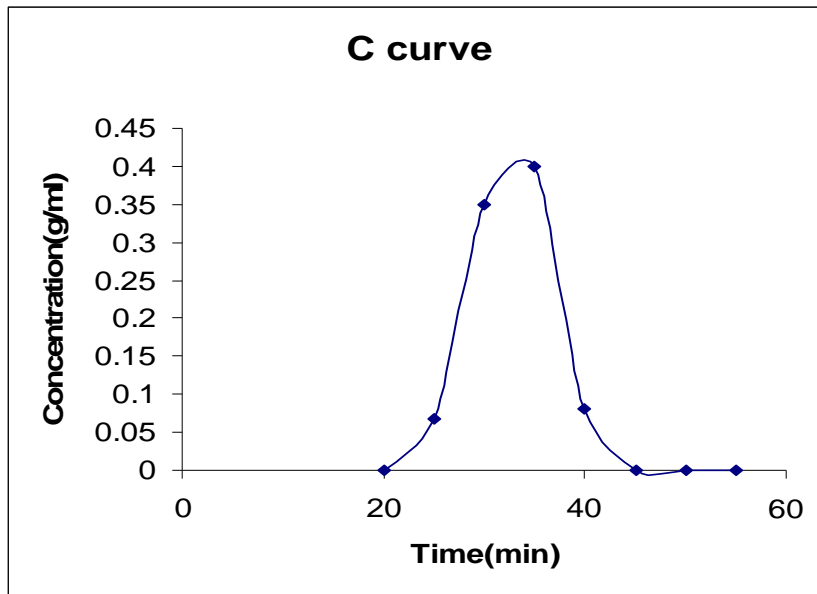


Figure 4.1 a. C curve for the trickle bed reactor using the scrubber as sample collector without water. **b.** Perfect pulse input representation compared to the pulse response for this configuration.

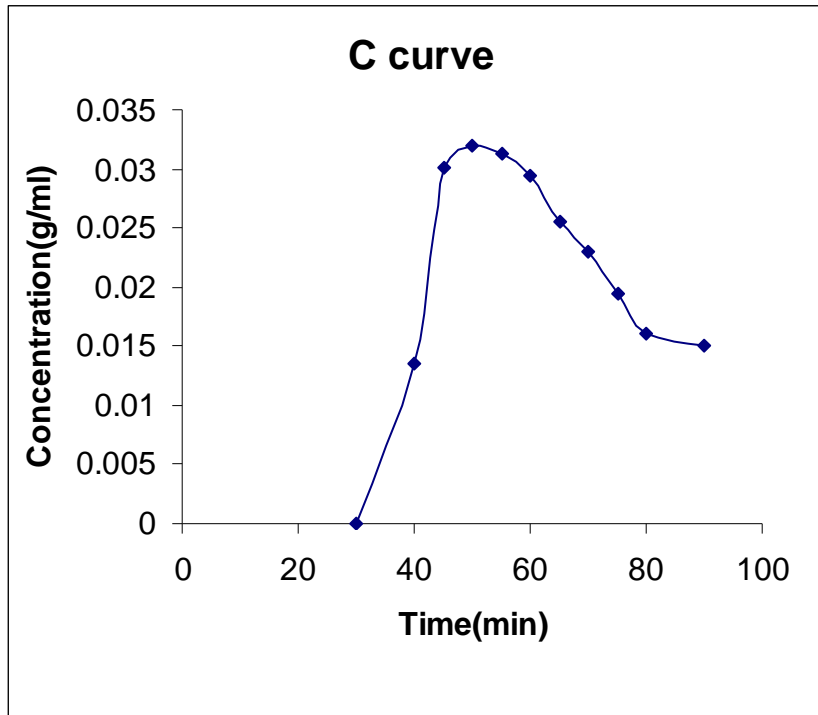


Figure 4.2 C curve using the scrubber with water as sample collector

When comparing Figures 4.1 and 4.2 it is noticeable that after injecting the tracer into the pump inlet the configuration using the scrubber with water as the sample collector took almost twice the time for the initial appearance of the tracer concentration. For this reason, the configuration using the scrubber without water as sample collector was selected for this study in order to have several samples produced per day and follow the catalyst deactivation closely.

It was mentioned on the literature review that the Peclet number N_{pe} is the parameter by which the residence time distribution is described. Figure 4.3 shows the variation of the Peclet number with superficial velocity for different particle diameter. For this graph the Peclet number calculation was

based on the Hochman and Effron correlation which it was recommended for hydrocarbon systems. As it was expected the Peclet number for this system had a small value as a consequence of the mixing and axial dispersion along the trickle bed reactor.

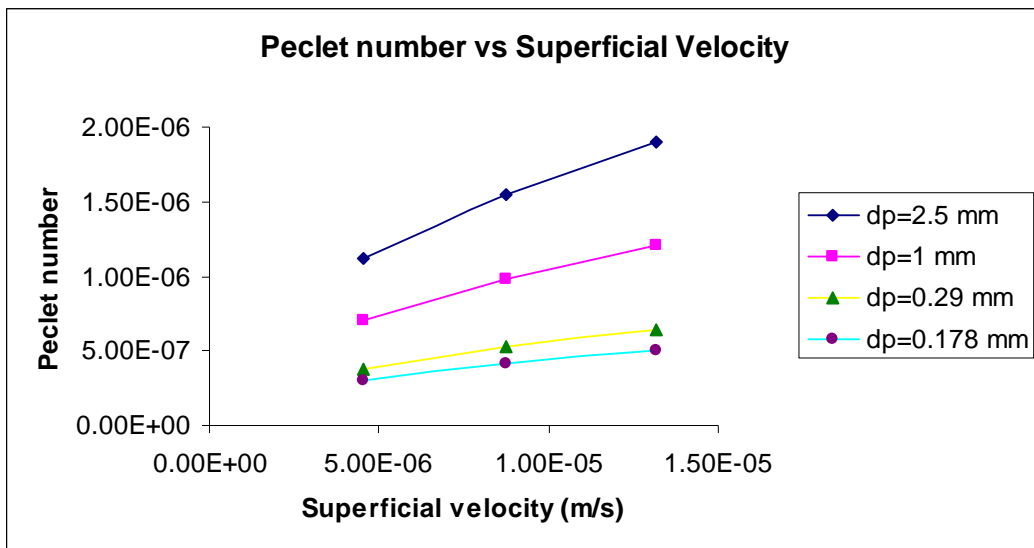


Figure 4.3 Peclet number vs Superficial velocity

4.2 Reactor Operation Improvement

4.2.1 Pressure and Temperature Management

In order to evaluate the system conditions, specifically the pressure and temperature settings, an initial hydrotreating experiments were conducted. The temperature profile across the reaction zone was also characterized.

The reactor was operated with a flow rate of 0.1 ml/min with a temperature of 360°C and a pressure of 3 MPa. Every 24 hours period, samples were collected consistently as follow: one sample overnight (12 hours period)

and two samples taken during the day (every 6 hours period). Results of measuring sulphur and nitrogen content in the product samples are shown in Table 4.1. The table shows that the sulphur and nitrogen contents in the samples collected during the day were higher than the content of nitrogen and sulphur in the samples collected overnight.

The discrepancy was attributed to the sample collection procedure and system. Samples collected during the day were obtained every six to eight hours and samples collected after the reactor had run overnight ten to twelve hours, during this time the collector was not emptied. The sample collection system did not have pressure compensation, and the collection of samples during the day and the emptying of the collector resulted in a decrease of the reactor system pressure. This effect was not meaningful for overnight samples because the sample was collected without emptying the collector for a period of at least ten hours. In other words, pressure lost during day sample collection causes a drop in sulphur and nitrogen conversion and as a consequence differences between overnight samples and day samples were visible.

For this reason future experiments had a pressure compensation system added to the collector in order to prevent pressure loss each time samples were collected.

Table 4.1 Nitrogen and sulphur content comparison night and day samples.

Sample	N(ppm*10) Overnight samples	N(ppm*10) Day samples	S(ppm*10) Overnight samples	S(ppm*10) Day samples
30-Sep	5.905	7.491	10.745	33.001
01-Oct	6.959	7	12.224	30.695
02-Oct	7.001	6.75	11.169	25.839
03-Oct	6.873	6.893	12.591	25.892
04-Oct	7.218	2.282	12.691	18.947
05-Oct	2.798	2.769	8.523	19.818
06-Oct	3.409	3.552	7.563	14.664
07-Oct	3.122	4.877	10.5	15.527

The temperature profile along the catalyst bed (Figure 4.3) was measured with a movable thermocouple. The first temperature profile was performed without a radiation shield. From this profile, it is notable that the temperature along the catalyst bed increased from the bottom to the top of the catalyst bed. Also, the difference between the bottom of the catalyst bed (the lowest temperature along the catalyst bed) and the furnace temperature was around 60°C. The second temperature profile was performed with a copper shield while the third temperature profile was performed with an aluminum shield. When comparing the two shields it is obvious that the aluminum shield performed better with regards to maintaining a uniform

temperature along the catalyst bed, with only a 2°C difference between the top and bottom of the bed. Also, the temperature difference between the furnace and the catalyst bed was reduced to around 20°C. For all future experiments, the aluminum shield was selected in order to maintain a uniform temperature along the catalyst bed.

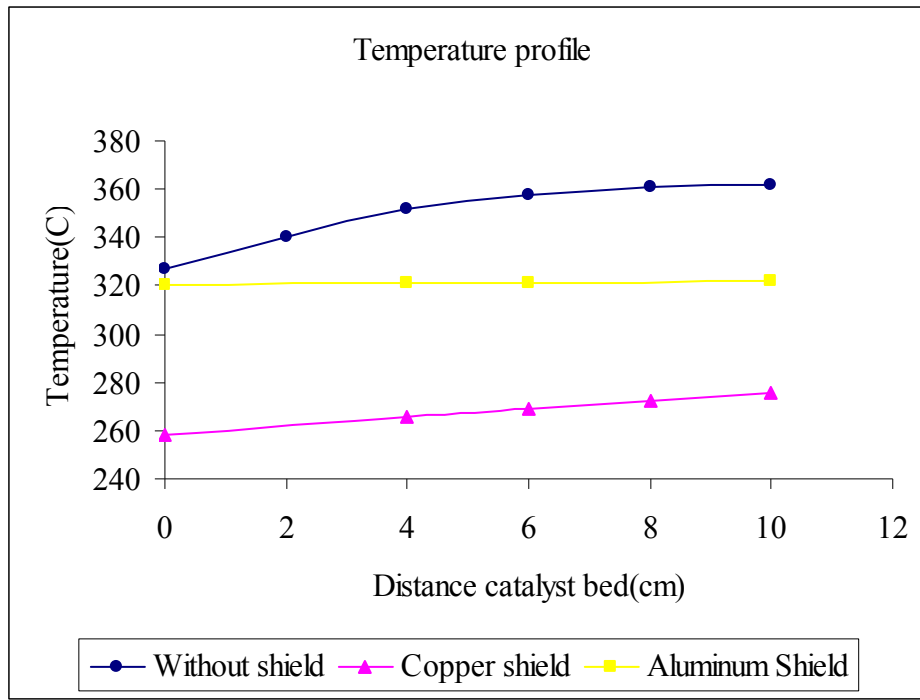


Figure 4.4 Temperature profile along the catalyst bed with different shields

Figure 4.5 shows the differences in configuration between the reactor with an aluminum jacket and with the copper jacket. For both configurations, the jacket and the reactor wall were as close as possible leaving just a small gap for the thermocouple. From this figure, it is visible that the aluminum jacket occupies all the space between the reactor and the oven walls. This configuration was the solution to the radiation and convection problems,

giving as a result a more uniform temperature profile along the reactor. Meanwhile, the copper shield configuration did not fill the space between the reactor and the oven walls. As a consequence, radiation problems were solved but convection still an issue, giving results less accurate for the temperature profile than the aluminum configuration.

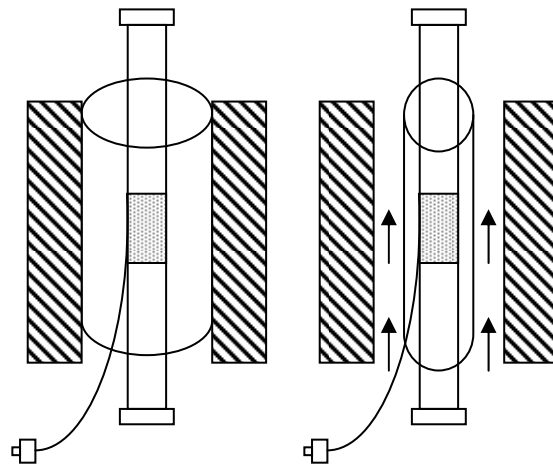


Figure 4.5 Differences in configuration between the reactor with an aluminum jacket (on the left) and with the copper jacket (right side).

4.3 Kinetics of Sulphur and Nitrogen Removal

In this study kinetic experiments were conducted by varying one variable and fixing two operating variables in order to collect data from which kinetic parameters were calculated. Operating variable effects were measured through the removal of sulphur and nitrogen from the light gas oil feed. The conversions of sulphur and nitrogen from the feed were defined as:

$$\%HDS, HDN = \frac{(S_f, N_f) - (S_p, N_p)}{S_f, N_f} \times 100 \quad (4.1)$$

Where S_f and N_f are the sulphur and nitrogen content in the feed and S_p and N_p are the sulphur and nitrogen content in the product.

4.3.1 Effects of Liquid Hourly Space Velocity and Temperature on HDS and HDN

The effect of space velocity on the sulphur and nitrogen removal from the light gas oil feed was studied in a range between 1-3 h⁻¹ at a fixed temperature of 315°C, a pressure of 3 MPa and hydrogen/oil ratio of 500ml/ml. Figure 4.6 shows the removal of sulphur and nitrogen versus liquid hourly space velocity. It is evident that the conversion of sulphur and nitrogen compounds decreased as liquid hourly space velocity increased. This behavior was anticipated since LHSV is the inverse of the oil feed contact time with the catalyst, which implies that increasing the LHSV will reduce the conversion since the reaction time decreases.

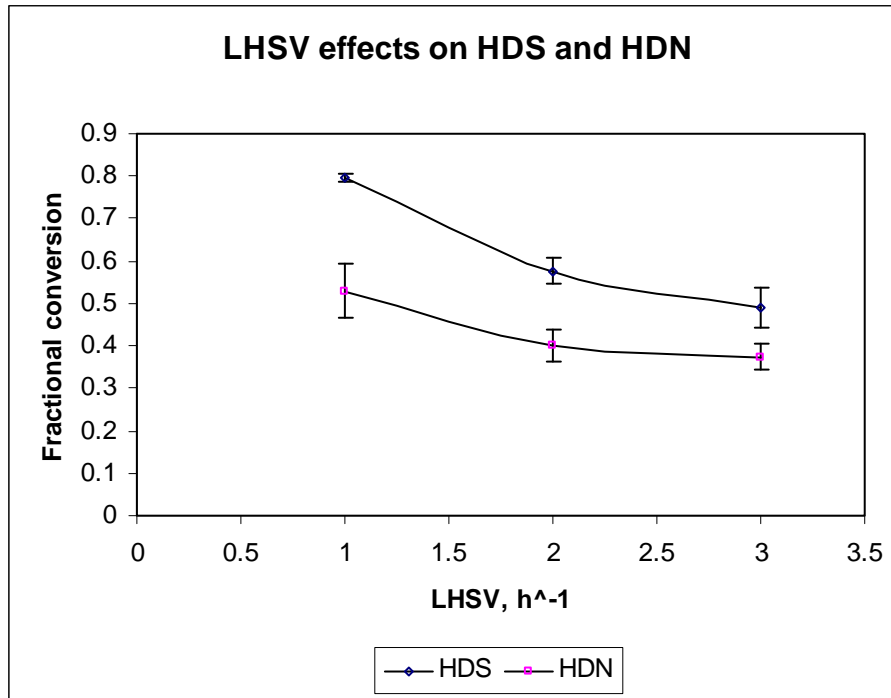


Figure 4.6 LHSV effects on HDS and HDN at 315°C, 3 MPa and hydrogen/oil ratio of 500 ml/ml.

The effect of temperature on the sulphur and nitrogen conversion from the light gas oil was studied by various temperatures in a range from 315-345°C. All other parameters such as pressure, liquid hourly space velocity and hydrogen/gas oil ratio were constant. Figure 4.7 shows the changes on sulphur and nitrogen conversion in relation to changes in temperature. It is evident from these results that as the temperature increased the quantities of sulphur and nitrogen removed from the feed also increased. It was also found that at every temperature, the conversion of sulphur compounds was greater than conversion of nitrogen compounds. This behavior was also identical during LHSV changes at fixed temperature and pressure.

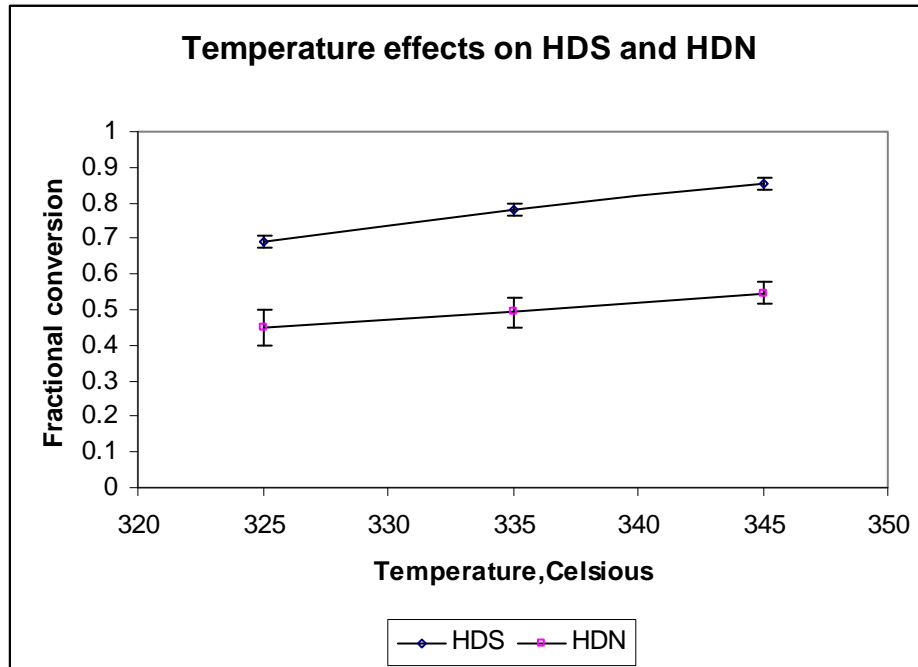


Figure 4.7 Temperature effects on HDS and HDN at 2 h^{-1} , 3MPa and hydrogen/oil ratio of 500 ml/ml.

Botchwey et al [27], presented results that are in agreement with this study, specifically that the removal of sulphur and nitrogen compounds decreases as LHSV increases and as temperature decreases. Furthermore, they established that there is a point at which a temperature increase does not affect the sulphur conversion but nitrogen removal continues to increase. Also in this study, it is observed that sulphur selectivity increases as LHSV increases.

From the data obtained through this study, it should be also noted that the effects of LHSV on sulphur removal were more prominent than the effect of temperature. Similar behavior was observed at low temperatures by

Abdul-Halim et al [28] who reported that LHSV had a greater influence on the sulphur removal than temperature.

Power law model have been used in numerous studies to obtain kinetic data due to their simplicity [9, 29] . For this reason, a power law model was used to describe the sulphur and nitrogen removal from light gas oil as shown below by Equation (4.2).

$$\frac{1}{n-1} \left[\frac{1}{C_p^{n-1}} - \frac{1}{C_f^{n-1}} \right] = \frac{k}{LHSV} \quad (4.2)$$

n =order of reaction.

C_p = Sulphur or nitrogen concentration in the hydrotreated product.

C_f =Sulphur or nitrogen concentration in the feed.

k = apparent rate constant.

$LHSV$ = liquid hourly space velocity.

The reaction order, n , was found by the best fit of our experimental results.

The different equations for diverse reaction order are shown in the Table 4.2 which also shows the fitting of the experimental data to the Equation

4.2. It is noticeable from the different R-squared values that the best fit of the experimental data for the HDS and HDN of the light gas oil correspond to a first reaction order, $n=1$. Figure 4.8 and Figure 4.9 shows the fitting of

the experimental data to a first order reaction for sulphur and nitrogen removal.

Table 4.2 Different reaction order equations and their R-square values

Reaction order(n)	Equation	R-sq for nitrogen	R-sq for sulphur
1	$\ln\left(\frac{C_f}{C_p}\right) = \frac{k}{LHSV}$	0.9529	0.9989
1.5	$2\left[\frac{1}{C_p^{0.5}} - \frac{1}{C_f^{0.5}}\right] = \frac{k}{LHSV}$	0.9417	0.9884
2	$\left[\frac{1}{C_p} - \frac{1}{C_f}\right] = \frac{k}{LHSV}$	0.9406	0.9818

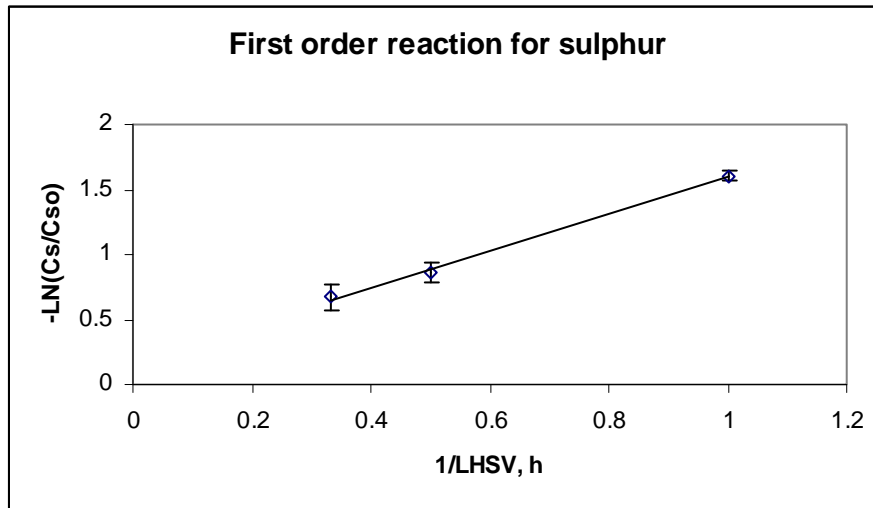


Figure 4.8 Fit of experimental data to the power law model for sulphur removal under the following conditions: LHSV between 1-3h⁻¹, temperature of 315°C, pressure of 3 MPa and hydrogen/oil ratio of 500ml/ml. First order reaction.

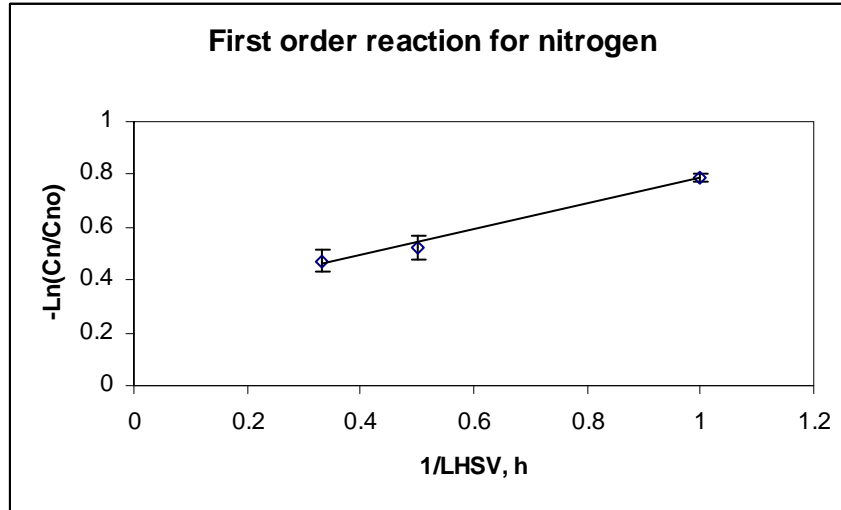


Figure 4.9 Fit of experimental data to the power law model for nitrogen removal under the following conditions: LHSV between 1-3h⁻¹, temperature of 315°C, pressure of 3 MPa and hydrogen/ oil ratio of 500ml/ml. First order reaction.

The rate constant is expressed with the Arrhenius equation (4.3):

$$k_0 \exp\left(\frac{-Ea}{RT}\right) = k \quad (4.3)$$

k_0 = Arrhenius constant.

Ea = Activation energy.

T = Temperature.

R = Gas constant.

k = Rate constant.

The Arrhenius plots for both nitrogen and sulphur reactions are shown in Figure 4.10 The activation energy values for HDN and HDS determined by the Arrhenius plot were 32kJ/mol and 76kJ/mol respectively.

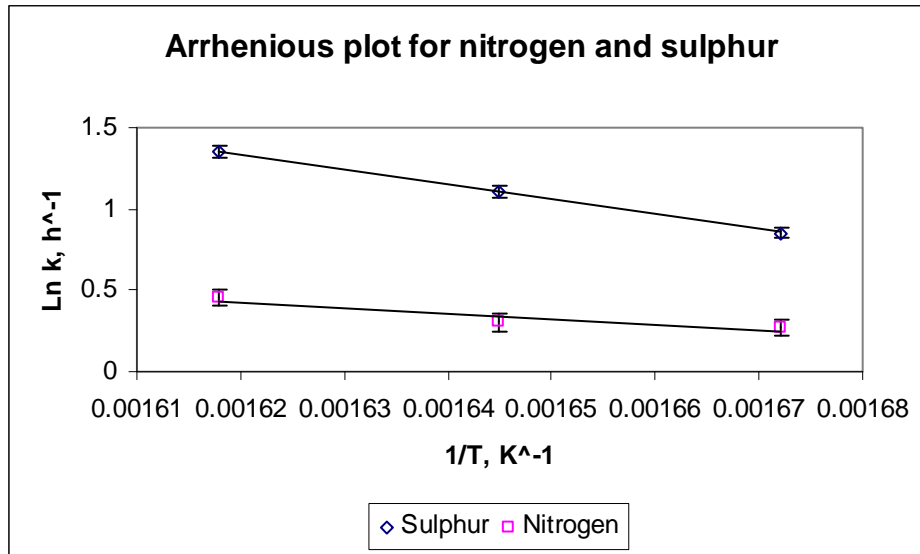


Figure 4.10 Arrhenius plot For HDS and HDN.

4.4 Arsenic introduction to the system

In order to verify a successful doping of arsenic in the feed and subsequently its introduction on the experimental system, 100 ppm of arsenic added to light gas oil feed (using triphenylarsine) was pumped into the trickle bed reactor system. SEM/EDX studies were done in the spent catalyst with the purpose of evaluating the cross section of the catalyst pellet. A picture of this characterization is shown in Figure 4.11. In this figure, points 1-4 were specific points of study in the pellet cross section with the purpose of analyzing its arsenic content. Table 4.3 shows the results of arsenic content for each point analyzed on the catalyst pellet. It is obvious that the highest amounts of the arsenic compound were found at the edge of the catalyst pellet.

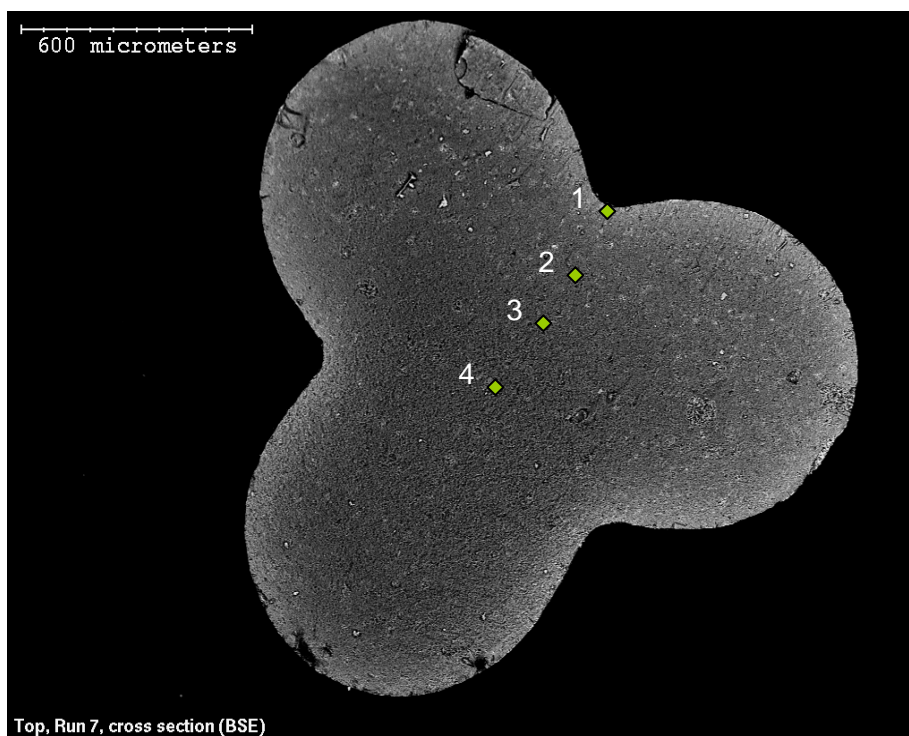


Figure 4.11 SEM/EDX picture of the cross section of a spent catalyst pellet.

Table 4.3 Arsenic content at different points of the cross section of the catalyst pellet

Position	As(Wt%)
1	5.1
2	2.9
3	2.1
4	0

Numerous studies have been reported on hydrodemetallation reactions of vanadium and nickel compounds in petroleum [6-7, 30-32]. Results [6, 30] have shown that there are two dominant patterns of metal distribution in spent catalyst pellets. One is a uniform distribution, which is typical for nickel deposition on a catalyst with large pores. The other is a U- shaped distribution

with maximum deposition at the edges, which is typical for vanadium on small pore catalyst pellets. The metal distribution profile varies with the reactivity and diffusivity of the metal compounds involved [6]. The higher the reactivity of the metal compounds, the greater the ratio of the chemical reaction rate to the diffusion rate, therefore, the metals are more likely to deposit on the outer edge of catalyst pellets. In the current study the deposition of arsenic on the NiMoS catalyst has a U-shaped distribution, which indicates that under the current reaction conditions, the reaction rate of triphenylarsine is faster than its diffusion rate of the NiMoS catalyst.

With the aim of studying the arsenic profile in the catalyst bed, neutron activation analysis was done to the catalyst bed separated in three parts: top, middle and bottom. Results of a pellet measurement from each part are shown in Table 4.4. From this result, it is evident that arsenic accumulation occurs at the top of the catalyst bed. This behavior was expected since the literature [33] reveals that in naphtha hydrotreaters most of the arsenic contamination is present at the top of the reactor and even suggest uploading carefully in order to replace just the contaminated part.

Table 4.4 Arsenic content in the top, middle and bottom of catalyst bed.

Position	Mass (mg)	As (wt%)
Top	72.0	6.80
Middle	77.2	2.95
Bottom	79.5	0.220

4.5 Activity Changes

In order to study the effects of arsenic on a commercial NiMo catalyst an investigation of the effect of arsenic loading on hydrotreating conversion was performed. Changes in the activation energy values and in the extent of the removal of nitrogen and sulphur were significant. Catalyst deactivation experiments in the micro trickle reactor were made by pumping a light gas oil feed with the addition of triphenylarsine to get the equivalent of 100 ppm of arsenic.

Changes in the catalyst behavior were evaluated through the activation energy values calculated before and after arsenic was introduced. For these replicated experiments the intake of arsenic was done running light gas oil with 100 ppm of arsenic per 6 days with a LHSV of 2 h⁻¹

Results for the activation energy values of two runs are shown in Table 4.5.

Table 4.5 Comparison between activation energy values before and after arsenic intake on replicated experiments.

	Run 8		Run7	
	Activation Energy (J/mol)		Activation Energy (J/mol)	
	Before As	After As	Before As	After As
HDS	68395	34177	76348	42290
HDN	36456	21034	32753	31744

From the results presented in the above table, it can be seen that for both HDS and HDN, activation energy values decreased with the presence of arsenic in the feed. This result may suggest that the diffusion limitations were becoming more severe with the presence of arsenic with time on stream. A study by Massagutov et al [34], on the effect of diffusion limitations upon apparent activation energy with a vacuum gas oil, shows the same behaviour, where increasing diffusion limitations caused a decrease in activation energy values. The effects of diffusional resistances on the activation energy have been illustrated in various studies, where the observed activation energy for a diffusion limited reaction is claimed to be approximately one half the true value.

With the purpose of evaluating the effect of arsenic on the catalyst performance, the results of HDS and HDN as a function of time on stream are shown in Figure 4.12 and Figure 4.13. For this evaluation the reactor and catalyst was stabilized for 5 days, after that a light gas oil with 100 ppm

of arsenic content was run for 14 days with a LHSV of 1 h^{-1} and a T of $315 \text{ }^\circ\text{C}$. A declining fractional conversion of sulphur and nitrogen is noticeable with increased time on stream. It is remarkable that for nitrogen conversion the decreasing trend is less pronounced than for sulphur conversion. This behaviour is also shown in the Table 4.6, where conversion of nitrogen and sulphur decreased after arsenic intake at different LHSV. It is also clear that the arsenic effects are more dramatic on sulphur conversion. This result may suggest that the incorporation of arsenic mainly affects the active site for HDS reactions.

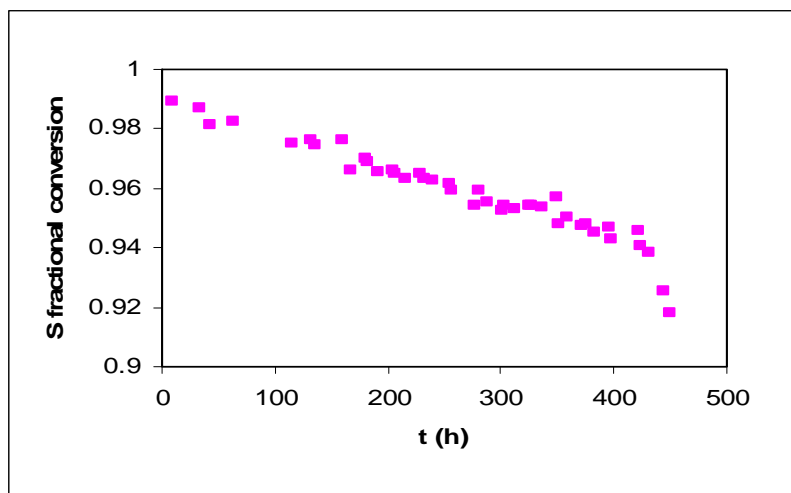


Figure 4.12 Sulphur conversion as a function of time on stream. Reaction conditions: $T=315^\circ\text{C}$, $P=3 \text{ MPa}$, $\text{LHSV}=0.08 \text{ h}^{-1}$, $\text{H}_2/\text{oil ratio}=500\text{ml/ml}$. Feed= LGO + 100 ppm of arsenic.

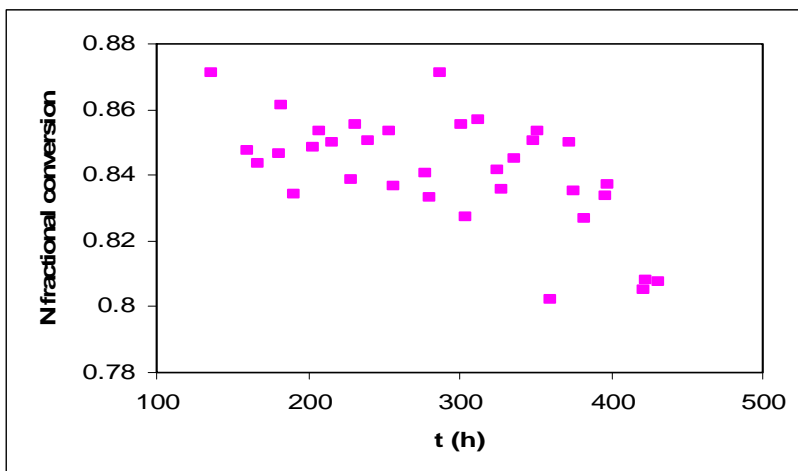


Figure 4.13 Nitrogen conversion as a function of time on stream. Reaction conditions: T=315°C, P=3 MPa, LHSV= 0.08 h⁻¹, H₂/oil ratio=500ml/ml. Feed= LGO + 100 ppm of arsenic.

Table 4.6 Arsenic effects on sulphur and nitrogen conversion at different LHSV

LHSV (h ⁻¹)	Sulfur conversion (%)		Nitrogen conversion (%)	
	Before As	After AS	Before AS	After AS
1	80	65	39	36
2	64	50	32	30
3	59	41	30	29

Previous studies in molecular simulation related to the incorporation of arsenic to the NiMoS catalyst illustrate that arsenic adsorption can occur on both the metal edge Ni (100) Mo-edge (Ni-edge) surface and at the sulphur edge S- sites on the Ni (100) S-edge. Yang et al [2], used density functional theory for studying arsenic poisoning of NiMoS hydrotreating catalysts, by comparing the adsorption energy calculations (see Table 4.7) they conclude that the adsorption of (C₆H₅)₃As) is favoured on both Ni

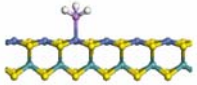
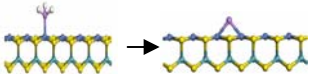
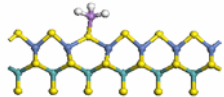
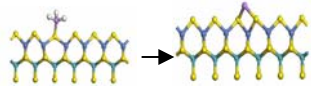
(100) Mo- and Ni (100) S-edge. However, after the organoarsenic molecules have adsorbed on the edge surfaces, dissociation on a Ni (100) S-edge surface is energetically favoured.

It is known that NiMoS catalysts are superior to CoMoS for hydrogenation (HYD) and HDN, while the opposite is true for HDS. The different behavior of the catalysts arises from their different edge surface structures. The absence of bare metal sites (like those on the metal edge of NiMoS) on CoMoS edge surface may explain its low activity in HYD and HDN.

A recent DFT study by Moses et al [35] on the hydrogenation and direct desulfurization reaction pathway in thiophene hydrodesulfurization over MoS₂ catalysts at realistic conditions shows that hydrogenation is easier on the Mo edge of MoS₂, while S–C scission can only occur on the S edge.

Knowing that the hydrogenation is easier at the metal edge of the catalysts and that the S-C scission occurs at the S edge, together with the fact that from the experimental data results it is evident that the arsenic mainly affects the conversion of sulfur compounds. These results indicate that arsenic prefers mainly the S edge of the catalysts at the real reaction conditions affecting the HDS activity of the NiMoS/Al₂O₃ catalyst.

Table 4.7 Comparison between arsenic adsorption and dissociation energies at different edges

Edge	Configuration	$(C_6H_5)_3As$
Metal		-2.11 eV
Metal		+1.24 eV
Sulfur		-1.21 eV
Sulfur		0.06 eV

Chapter V

CONCLUSIONS

1. Improvement to the reactor system was made in order to successfully prevent pressure drop during sample collection and to have a uniform temperature profile along the trickle bed reactor system. In order to achieve these desired parameters, a pressure compensation system and an aluminum coating were installed in the trickle bed reactor system.
2. The HDS and HDN of the light gas oil using a NiMo- γ Al₂O₃ was evident under the following conditions: a temperature range of 315-345 °C, a liquid hourly space velocity between 1-3 h⁻¹, a pressure of 3 MPa and a hydrogen to oil ratio of 500 ml/ml. Kinetics over this commercial catalyst followed first order reaction for both, HDS and HDN of the light gas oil, having activation values of 76 kJ/mol and 32 kJ/mol respectively.
3. After the system saturation, arsenic was successfully introduced into the system. SEM/EDX analysis of the catalyst pellet determined a U profile of arsenic diffusion into the pellet. Neutron Activation analysis to the catalyst bed indicated that most of the arsenic was at the top of the catalyst bed as it was expected.

4. After arsenic introduction to the system, a comparison between activation energy values for HDS and HDN on similar experiments revealed that activation energy values decreased for both HDS and HDN from 68kj/mol to 34kj/mol and from 36 kj/mol to 21 kj/mol respectively, which may suggest diffusion problems due to pore plugging.
5. A declining fractional conversion of sulphur and nitrogen was noticeable with arsenic on stream. For sulphur conversion, decreases of up to 30 percent were found after arsenic was added. The decrease for nitrogen conversion was significantly less, with a maximum of 8 percent after arsenic addition. In summary, for nitrogen conversion the decreasing trend is less pronounced than for sulphur conversion. This result may suggest that the incorporation of arsenic mainly affects the active site for HDS reactions.

Bibliography

1. Kwak, S., *Hydrotreating heavy oils over a commercial hydrometallation catalyst*, in *Department of chemicals and fuels engineering*. 1994, University of Utah.
2. Shaofeng, Y., J. Adjaye, W. McCaffrey, and A. Nelson, *Density functional theory (DFT) study of arsenic poisoning of NiMoS*. *Journal of molecular catalysis A*, 2010. **chemical 321**: p. 83-91.
3. Bhan, O.K., *Arsenic Removal Catalyst and Process for Making Same*. 2004: United States.
4. Stigter, J.B., H.P.M. de Haan, R. Guicherit, C.P.A. Dekkers, and M.L. Daane, *Determination of Cadmium, Zinc, Copper, Chromium and Arsenic in Crude Oil Cargoes*. *Environmental Pollution*, 2000. **107**: p. 451-464.
5. Nielsen, B. and J. Villadsen, *Poisoning of Nickel Catalysts by Arsenic*. *Applied Catalysis*, 1984. **11**: p. 123-138.
6. Isaza Nunez, M., Z. Pachon, V. Kafarov, and D. Resasco, *Deactivation of NiMo/Al₂O₃ catalyst aged in a commercial reactor during the hydrotreating of deasphalted vacuum residuum*. *Applied Catalysis A:General*, 2000. **199**: p. 263-273.
7. Callejas, M. and M. Martinez, *Hydroprocessing of a Maya Residue. Intrinsic kinetics of sulfur, nitrogen, nickel and vanadium removal reactions*. *Energy and Fuels*, 1999. **13**: p. 629-636.
8. Marafi, A., A. Stanislaus, A. Hauser, and K. Matsushita, *An investigation of the deactivation behavior of industrial Mo/Al₂O₃ and Ni-Mo/Al₂O₃ catalysts in hydrotreating Kuwait atmospheric residue*. *Petroleum Science and Technology*, 2005. **23**: p. 385-408.
9. Adjaye, J., K. Dalai, and K. Bej, *Kinetics of Hydrodesulfuration of Heavy Gas Oil Derived From Oil-Sands Bitumen*. *Petroleum Science and Technology*, 2002. **20**(7 and 8): p. 867-877.
10. Maurice, V., Y.A. Ryndin, G. Bergeret, L. Savary, J.P. Candy, and J.M. Basset, *Influence of the Dispersion of Metallic Particles on the Reaction of Triphenylarsine with Alumina-Supported Nickel*. *Journal of catalysis*, 2001. **204**: p. 192-199.
11. Gray, M.R., *Upgrading Petroleum Residues and Heavy Oils*. Marcel Dekker 1994.

12. Owuso-Boakye, A., *Two-stage aromatics hydrogenation of bitumen-derived light gas oil*, in *Department of chemical engineering*. 2005, University of Saskatchewan.
13. Gupta, v., *Cracking and heteroatom removal from hydrocarbons using natural zeolites*, in *Department of chemical engineering*. 2008, University of Alberta.
14. Furimsky, E., *Catalysts for upgrading Heavy Petroleum Feeds*. Studies in Surface Science and Catalysis, ed. G.Centi. 2007, Amsterdam, The Netherlands: Elsevier.
15. Muegge, B.D., *Basic studies in deactivation of hydrotreating catalyst by coke*, in *Department of chemical engineering*. 1991, University of Utah.
16. Gianetto, A. and P. L.Silveston, *Multiphase Chemical Reactors*. 1986, United States of North America: Hemisphere Publishing Corporation.
17. Butt, J., *Reaction kinetics and reactor design*. Second ed, ed. M. Dekker. 2000, New york.
18. Shah, Y., *Gas-Liquid-Solid Reactor Design*. 1979, United States of America: McGraw-Hill International book company.
19. Mears, D.E., *Chemical Reaction Engineering II*. 1974.
20. Paraskos, J., J. Frayer, and Y. Shah, *I&EC Process Design Dev*. 1975. **14**.
21. Montagna, A.A., Y. Shah, and Paraskos, *I&EC Process Design Dev*. 1977. **16**.
22. Puranik, S. and A. Vogelpohl, *Chem.Eng.Sci*. 1974. **29**.
23. Michell, R.W. and I.A. Furzer, *Chem. Eng. J*. 1972. **4**.
24. Hochman, J.M. and E. Effron, *I&EC Fund*. Vol. 8. 1969.
25. Satterfield, C., *Mass Transfer in Heterogeneous Catalysis*. 1981, Florida: Robert E.Krieger Publishing Company, Inc.
26. Fogler, H.S., *Elements of Chemical Reaction Engineering*. Third ed. 2002, New Jersey: Prentice Hall International Series.
27. Botchwey, C., K. Dalai, and J. Adjaye, *Kinetics of Bitumen-Derived Gas Oil Upgrading Using a Commercial NiMo/Al₂O₃ Catalyst*. The Canadian Journal Of Chemical Engineering, 2004. **82**: p. 478-487.

28. Abdul-Halim, A., H. Hussain, H. Karim, and N. Ihsan, *Hydrotreating of qaiyarah deasphalted residue*. Fuel, 1988. **67**: p. 36.
29. Ferdous, D., K. Dalai, and J. Adjaye, *Hydrodenitrogenation and hydrodesulphuration of heavy gas oil using NiMo/Al₂O₃ catalyst containing phosphorus: experimental and kinetics studies*. The Canadian Journal Of Chemical Engineering, 2005. **83**.
30. McEvoy, J.E., T.H. Milliken, and G.A. Mills, *Distribution of metal contaminants on cracking catalysts*. Industrial and Engineering Chemistry, 1957. **49**(5): p. 865-868.
31. Maity, S., J. Ancheyta, F. Alonso, and J. Vazquez, *Study of accelerated deactivation of hydrotreating catalysts by vanadium impregnation method*. Catalysis Today, 2007. **130**: p. 405-410.
32. Stanislaus, A., A. Marafi, and M. Almarri, *The usage of high metal feedstock for the determination of metal capacity of ARDS catalyst system by accelerated aging tests*, in *Catalysis Today*. 2008. p. 395-404.
33. Homan Free, H. *Catalyst Deactivation [HVGO's and lighter feeds]*. Catalysis courier **17**.
34. Massagutov, R., G.M. Mulinich, T.S. Kirillou, and G.A. Berg, *Kinetics of high-sulphur distillate hydrotreating*, in *7th World Pet. Congr. Proc.* 1967. p. 177-183.
35. Moses, P.G., B. Hinnermann, H. Topsoe, and J. Narskou, *The hydrogenation and direct desulfurization reaction pathway in thiophene hydrodesulfurization over MoS₂ catalysts at realistic conditions: a density functional study*. Journal of catalysis, 2008. **260**: p. 202-203.